tiretroviral therapeutics for HIV infection," 2nd ed., eds. by Merigan T. C., Bartlett J. G., Bolognesi D., Williams & Wilkins, Baltimore, 1999, pp. 751–780.
7) Alkhatib G., Combadiere C., Broder C. C., Feng Y., Kennedy P. E., Murphy P. M., Berger E. A., *Science*, **272**, 1955–1958 (1996).
8) Feng Y., Broder C. C., Kennedy P. E., Berger E. A., *Science*, **272**, 872–877 (1996).
9) Chan D. C., Fass D., Kim P. S., *Cell*, **89**, 263–273 (1997).
10) Walker D. K., Abel S., Comby P., Muirhead G. J., Nedderman A. N., Smith D. A., *Drug Metab. Dispos.*, **33**, 587–595 (2005).
11) Fujii N., Nakashima H., Tamamura H., *Expert Opin. Investig. Drugs*, **12**, 185–195 (2003).
12) Murakami T., Nakajima T., Koyanagi Y., Tachibana K., Fujii N., Tamamura H., Yoshida N., Waki M., Matsumoto A., Yoshie O., Kishimoto T., Yamamoto N., Nagasawa T., *J. Exp. Med.*, **186**, 1389–1393 (1997).
13) Tamamura H., Xu Y., Hattori T., Zhang X., Arakaki R., Kanbara K., Omagari A., Otaka A., Ibuka T., Yamamoto N., Nakashima H., Fujii N., *Biochem. Biophys. Res. Commun.*, **253**, 877–882 (1998).
14) Tamamura H., Hiramatsu K., Kusano S., Terakubo S., Yamamoto N., Trent J. O., Wang Z., Peiper S. C., Nakashima H., Otaka A., Fujii N., *Org. Biomol. Chem.*, **1**, 3656–3662 (2003).
15) Tamamura H., Hiramatsu K., Mizumoto M., Ueda S., Kusano S., Terakubo S., Akamatsu M., Yamamoto N., Trent J. O., Wang Z., Peiper S. C., Nakashima H., Otaka A., Fujii N., *Org. Biomol. Chem.*, **1**, 3663–3669 (2003).
16) Fujii N., Oishi S., Hiramatsu K., Araki T., Ueda S., Tamamura H., Otaka A., Kusano S., Terakubo S., Nakashima H., Broach J. A., Trent J. O., Wang Z., Peiper S. C., *Angew. Chem. Int. Ed.*, **42**, 3251–3253 (2003).
17) Tamamura H., Tsutsumi H., Masuno H., Mizokami S., Hiramatsu K., Wang Z., Trent J. O., Nakashima H., Yamamoto N., Peiper S. C., Fujii N., *Org. Biomol. Chem.*, **4**, 2354–2357 (2006).
18) Tamamura H., Ojida A., Ogawa T., Tsutsumi H., Masuno H., Nakashima H., Yamamoto N., Hamachi I., Fujii N., *J. Med. Chem.*, **49**, 3412–3415 (2006).
19) Tanaka T., Narumi T., Ozaki T., Sohma A., Ohashi N., Hashimoto C., Itotani K., Nomura W., Murakami T., Yamamoto N., Tamamura., *ChemMedChem*, **6**, 834–839 (2011).
20) Tamamura H., Tsutsumi H., Nomura W., Tanaka T., Fujii N., *Expert Opin. Drug Discov.*, **3**, 1155–1166 (2008).
21) Tamamura H., Hori A., Kanzaki N., Hiramatsu K., Mizumoto M., Nakashima H., Yamamoto N., Otaka A., Fujii N., *FEBS Lett.*, **550**, 79–83 (2003).
22) Tamamura H., Fujisawa M., Hiramatsu K., Mizumoto M., Nakashima H., Yamamoto N., Otaka A., Fujii N., *FEBS Lett.*, **569**, 99–104 (2004).
23) Tamamura H., Otaka A., Fujii N., *Curr. HIV Res.*, **3**, 289–301 (2005).
24) Zhao Q., Ma L., Jang S., Lu H., Liu S., He Y., Strick N., Neamati N., Debnath A. K., *Virology*, **339**, 213–225 (2005).
25) Mandai N., Schön A., Princiotto A. M., LaLonde J. M., Courter J. R., Soeta T., Ng D., Wang L., Brower E. T., Xiang S.-H., Kwon Y. D., Huang C.-C., Wyatt R., Kwong P. D., Freire E., Smith A. B. III, Sodroski J., *Structure*, **16**, 1689–1701 (2008).
26) Yamada Y., Ochiai C., Yoshimura K., Tanaka T., Ohashi N., Narumi T., Nomura W., Harada S., Matsuhita S., Tamamura H., *Bioorg. Med. Chem. Lett.*, **20**, 354–358 (2010).
27) Yoshimura K., Harada S., Shibata J., Hatada M., Yamada Y., Ochiai C., Tamamura H., Matsushita S., *J. Virol.*, **84**, 7558–7568 (2010).
28) Narumi T., Ochiai C., Yoshimura K., Harada S., Tanaka T., Nomura W., Arai H., Ozaki T., Ohashi N., Matsushita S., Tamamura H., *Bioorg. Med. Chem. Lett.*, **20**, 5853–5858 (2010).
29) Suzuki S., Urano E., Hashimoto C., Tsutsumi H., Nakahara T., Tanaka T., Nakanishi Y., Maddali K., Han Y., Hamatake M., Miyauchi K., Pommier Y., Beutler J. A., Sugiura W., Fuji H., Hoshino T., Itotani K., Nomura W., Narumi T., Yamamoto N., Komano J. A., Tamamura H., *J. Med. Chem.*, **53**, 5356–5360

(2010).
30) Suzuki S., Maddali K., Hashimoto C., Urano E., Ohashi N., Tanaka T., Ozaki T., Arai H., Tsutsumi H., Narumi T., Nomura W., Yamamoto N., Pommier Y., Komano J. A., Tamamura H., *Bioorg. Med. Chem.*, **18**, 6771–6775 (2010).
31) Mukai H., Hokari Y., Seki T., Takao T., Kubota M., Matsuo Y., Tsukagoshi H., Kato M., Kimura H., Shimonishi Y., Kiso Y., Nishi Y., Wakamatsu K., Munekata E., *J. Biol. Chem.*, **283**, 30596–30605 (2008).
32) Grinsztejn B., Nguyen B.-Y., Katlama C., Gatell J. M., Lazzarin A., Vittecoq D., Gonzalez C. J., Chen J., Harvey C. M., Isaacs R. D., Protocol 005 Team, *Lancet*, **369**, 1261–1269 (2007).
33) Wild C. T., Greenwell T. K., Matthews T. J., *AIDS Res. Hum. Retroviruses*, **9**, 1051–1053 (1993).
34) Alam S. M., McAdams M., Boren D., Rak M., Scearce R. M., Gao F., Camacho Z. T., Gewirth D., Kelsoe G., Chen P. J., Haynes B. F., *J. Immunol.*, **178**, 4424–4435 (2007).
35) Tam J. P., Yu Q., *Org. Lett.*, **4**, 4167–4170 (2002).
36) Louis J. M., Nesheiwat I., Chang L., Clore G. M., Bewlet C. A., *J. Biol. Chem.*, **278**, 20278–20285 (2003).
37) Bianch E., Finotto M., Ingallinella P., Hrin R., Carella A. V., Hou X. S., Schleif W. A., Miller M. D., Geleziunas R., Pessi A., *Proc. Natl. Acad. Sci. USA*, **102**, 12903–12908 (2005).
38) Nakahara T., Nomura W., Ohba K., Ohya A., Tanaka T., Hashimoto C., Narumi T., Murakami T., Yamamoto N., Tamamura H., *Bioconjugate Chem.*, **21**, 709–714 (2010).

Bioorganic & Medicinal Chemistry 21 (2013) 2518–2526

Contents lists available at SciVerse ScienceDirect

Bioorganic & Medicinal Chemistry

journal homepage: www.elsevier.com/locate/bmc

CD4 mimics as HIV entry inhibitors: Lead optimization studies of the aromatic substituents

Tetsuo Narumi [a], Hiroshi Arai [a], Kazuhisa Yoshimura [b,c], Shigeyoshi Harada [b,c], Yuki Hirota [a], Nami Ohashi [a], Chie Hashimoto [a], Wataru Nomura [a], Shuzo Matsushita [b], Hirokazu Tamamura [a,*]

[a] Institute of Biomaterials and Bioengineering, Tokyo Medical and Dental University, Chiyoda-ku, Tokyo 101-0062, Japan
[b] Center for AIDS Research, Kumamoto University, Kumamoto 860-0811, Japan
[c] AIDS Research Center, National Institute of Infectious Diseases, Shinjuku-ku, Tokyo 162-8640, Japan

ARTICLE INFO

Article history:
Received 22 January 2013
Revised 25 February 2013
Accepted 26 February 2013
Available online 7 March 2013

Keywords:
CD4 mimicry
Conformational change in gp120
HIV entry inhibitor
Envelope protein opener

ABSTRACT

Several CD4 mimics have been reported as HIV-1 entry inhibitors that can intervene in the interaction between a viral envelope glycoprotein gp120 and a cell surface protein CD4. Our previous SAR studies led to a finding of a highly potent analogue **3** with bulky hydrophobic groups on a piperidine moiety. In the present study, the aromatic ring of **3** was modified systematically in an attempt to improve its antiviral activity and CD4 mimicry which induces the conformational changes in gp120 that can render the envelope more sensitive to neutralizing antibodies. Biological assays of the synthetic compounds revealed that the introduction of a fluorine group as a *meta*-substituent of the aromatic ring caused an increase of anti-HIV activity and an enhancement of a CD4 mimicry, and led to a novel compound **13a** that showed twice as potent anti-HIV activity compared to **3** and a substantial increase in a CD4 mimicry even at lower concentrations.

© 2013 Published by Elsevier Ltd.

1. Introduction

The first step of HIV entry into host cells is the interaction of a viral envelope glycoprotein gp120 with the cell surface protein CD4.[1] Such a viral attachment process is an attractive target for the development of the drugs to prevent the HIV-1 infection of its target cells.[2] Several small molecules including BMS-806,[3] IC-9564[4] and NBDs[5] have been identified that inhibit the viral attachment process by binding to gp120. Recently, we and others have been exploring the potentials of NBDs-derived CD4 mimics as a novel class of HIV entry inhibitors (Fig. 1).[6–8]

Small molecular CD4 mimics identified by an HIV syncytium formation assay showed potent cell fusion and virus cell fusion inhibitory activity against several HIV-1 laboratory and primary isolates.[5] Furthermore, the interaction of CD4 mimics with a highly conserved and functionally important pocket on gp120, known as the 'Phe43 cavity', induces conformational changes in gp120,[9] a process which occurs with unfavorable binding entropy, leading to a favorable enthalpy change similar to those caused by binding of the soluble CD4 binding to gp120. These unique properties render CD4 mimics valuable not only for the development of entry inhibitors, but which also, when combined with neutralizing antibodies function as envelope protein openers-putatively, stimulants.[10]

The structure of the complex formed by NBD-556 (**1**) bound to the gp120 core from an HIV-1 clade C strain (C1086) was recently determined by X-ray analysis (PDB: 3TGS).[11] As expected with molecular modeling by us[8a] and others,[6a] NBD-556 binds with Phe43 cavity with its *p*-chlorophenyl ring inserted into the cavity, and in addition multiple contacts were observed, with Trp112, Val255, Phe382, Ile424, Asn425, Trp427, Gly473, and Val430 of gp120 were observed (Fig. 2). However, no obvious interaction with Arg59 of CD4 was observed, although the salt bridge formation between Arg59 of CD4 and Asp368 of gp120 is a critical interaction of the viral attachment.[12] Based on this binding model, several potent compounds were recently identified.[6c,7]

Prior to those studies, we performed structure–activity relationship (SAR) studies based on the modification of the piperidine moiety of CD4 mimics to interact with Val430 and/or Asp368. These resulted in the discovery of a potent compound **3** which has bulky hydrophobic groups on its piperidine ring, and shows significant anti-HIV activity and lower cytotoxicity than other known CD4 mimics.[8c] Our study of the docking of **3** into the Phe43 cavity of gp120 suggests that the cyclohexyl group of **3** can interact hydrophobically with the isopropyl group of Val430.

We hypothesized that the optimization of the aromatic ring of **3** would lead to an increase of antiviral activity and CD4 mimicry, the latter inducing the conformational changes in gp120. Here, we de-

* Corresponding author. Tel.: +81 3 5280 8036; fax: +81 3 5280 8039.
E-mail address: tamamura.mr@tmd.ac.jp (H. Tamamura).

0968-0896/$ - see front matter © 2013 Published by Elsevier Ltd.
http://dx.doi.org/10.1016/j.bmc.2013.02.041

scribe the systematic modification of the aromatic ring of **3** for further optimization to evaluate substituent effects on anti-HIV activity, cytotoxicity and CD4 mimicry.

2. Results and discussion

The co-crystal structure of **1** with the gp120 core revealed that the aromatic group of **1** binds to gp120 by several aromatic–aromatic and hydrophobic interactions (Fig. 2). In particular, hydrophobic space surrounded by the hydrophobic amino acid residues Trp112, Val255, Phe382, and Ile424 is likely to be affected by substituents at the *meta*- and *para*-positions of the aromatic ring, and consequently we decided to investigate substituents at these positions (Fig. 3).

Initially, we selected a chlorine or a methyl group to serve as the *para*-substituent of the aromatic group because CD4 mimic compounds such as **1** (NBD-556) with a *p*-chloro substituent, and because **3** showed significant anti-HIV activity compared to other substituents. Further, CD4 mimic structures such as **2** with a *p*-methyl substituent also showed potent anti-HIV activity and exhibits lower cytotoxicity than those with the *p*-chlorophenyl derivatives.[8a] Next, we chose several halogens including F, Cl and Br, to be the *meta*-substituent on the aromatic group since previous SAR studies revealed that the introduction of an appropriate group with an electron-withdrawing ability at the *meta*-position leads to an increase of binding affinity and antiviral activity.[6a] Furthermore, to investigate whether electron withdrawal and hydrophobicity of the *meta*-position are appropriate, the CD4 mimics with a *meta*-methyl substituent, which has electron-donating properties and is similar in size to bromine, were also synthesized. Finally, two piperidine scaffolds (the 2,2,6,6-tetramethylpiperidine **A** and the dicyclohexylpiperidine **B**) were combined with these aromatics via the oxalamide linker.

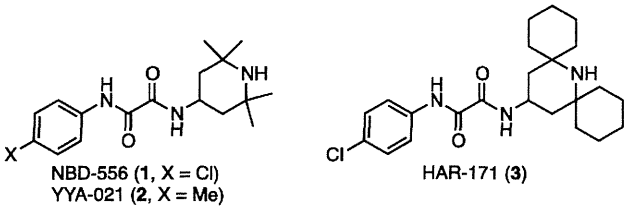

Figure 1. Structures of NBD-556 (**1**), YYA-021 (**2**) and HAR-171 (**3**).

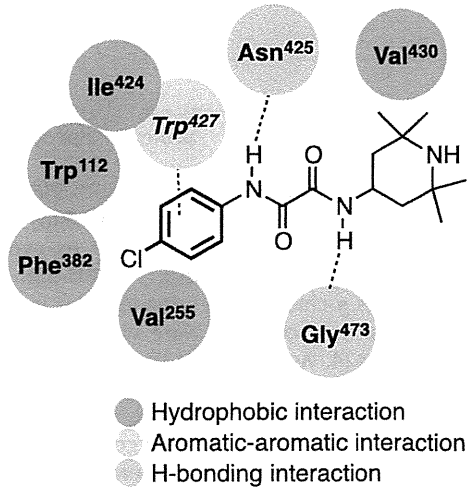

Figure 2. Major interactions between NBD-556 and Phe43 cavity of gp120.

2.1. Chemistry

The syntheses of novel compounds are depicted in Schemes 1 and 2. Starting from the appropriate aniline with *m*- and *p*-substituents, coupling with ethyl chloroglyoxylate in the presence of Et_3N gave the corresponding amidoesters **6a–c** and **7a–c**. Subsequently, microwave-assisted aminolysis[13] of **6a–c** and **7a–c** with commercially available 4-amino-2,2,6,6-tetramethylpiperidines afforded the desired compounds **8a–c** and **9a–c** (Scheme 1). A series of CD4 mimics with two cyclohexyl groups **13a–c** and **14a–c** were prepared from 2,2,6,6-tetramethylpiperidin-4-one **10** by the method previously reported,[8c] with slight modification (Scheme 2). Briefly, treatment of **10** with cyclohexanone in the presence of ammonium chloride gave a 2,6-substituted piperidin-4-one **11** via Grob fragmentation followed by intramolecular cyclization.[14] Reductive amination with *p*-methoxybenzyl amine, acidic treatment with TMSBr/TFA, and oxidative cleavage of *p*-methoxybenzyl group with cerium(IV) ammonium nitrates (CAN) furnished the corresponding 4-aminopiperidines (**12**) with higher yields and less burdensome purifications than the previous method. Finally, coupling of **12** with the corresponding esters **6a–c** and **7a–c** under microwave irradiation provided the desired compounds **13a–c** and **14a–c**.

2.2. Biological evaluation

The anti-HIV activity of the synthetic compounds was evaluated against an R5 primary isolate YTA strain. IC_{50} values were determined by the WST-8 method as the concentrations of the compounds that conferred 50% protection against HIV-1-induced cytopathogenicity in PM1/CCR5 cells. Cytotoxicity of the compounds based on the viability of mock-infected PM1/CCR5 cells was also evaluated using the WST-8 method. The assay results for compounds **8a–c** and **13a–c** with a *p*-chlorophenyl group are shown in Table 1. The parent compound **1** and compound **8a**,[6a] known as JRC-II-191, showed significant anti-HIV activities (IC_{50}

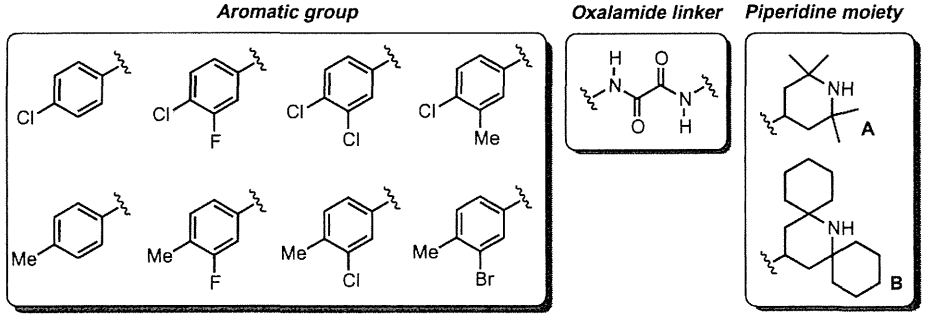

Figure 3. The structures of scaffolds in the design of novel CD4 mimics.

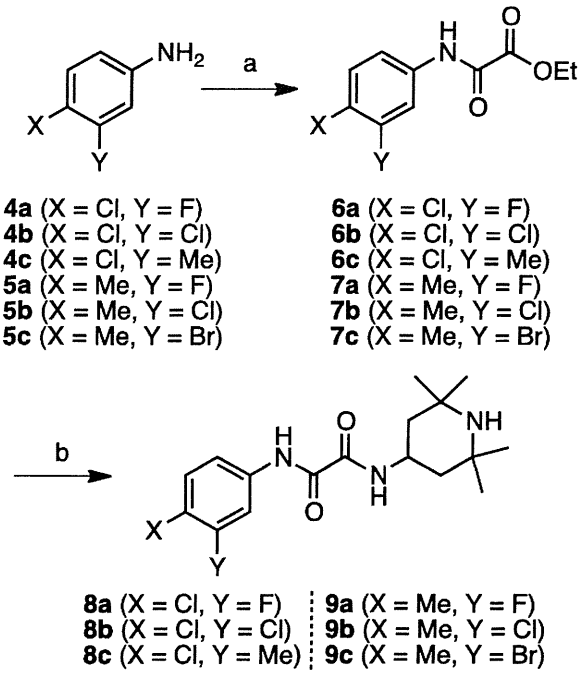

Scheme 1. Reagents and conditions: (a) ethyl chloroglyoxylate, Et_3N, THF; (b) 4-amino-2,2,6,6-tetramethylpiperidine, Et_3N, EtOH, 150 °C, microwave.

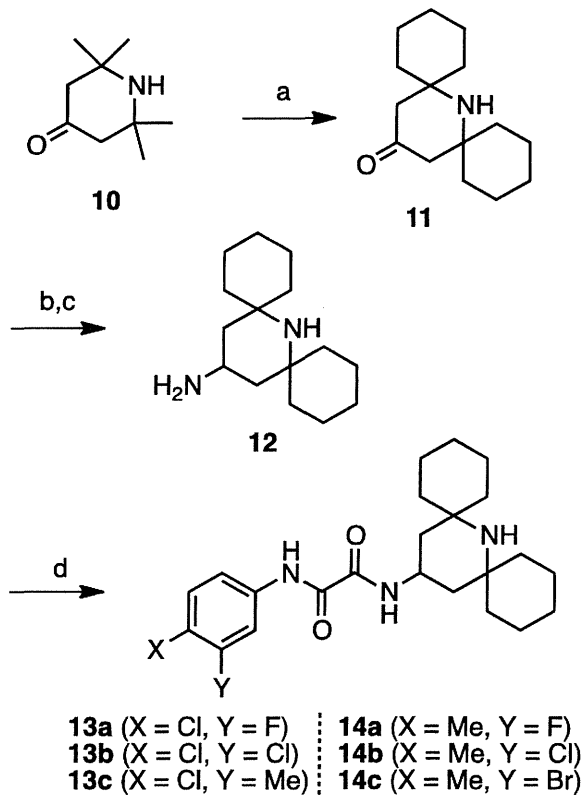

Scheme 2. Reagents and conditions: (a) cyclohexanone, NH_4Cl, DMSO, 60 °C; (b) *p*-methoxybenzylamine, $NaBH_3CN$, MeOH, then 1 M TMSBr in TFA; (c) CAN, CH_3CN/H_2O (v:v = 2:1); (d) **6** or **7**, Et_3N, EtOH, 150 °C, microwave.

of **1** = 0.61 μM and IC_{50} of **8a** = 0.32 μM). Compound **8b**[6a] having a *m,p*-dichlorophenyl group and compound **8c**[6a] (JRC-II-193) having a *p*-chloro-*m*-tolyl group showed moderate anti-HIV activity (IC_{50} of **8b** = 4.1 μM and IC_{50} of **8c** = 3.3 μM) but their potency was

Table 1
Anti-HIV activity and cytotoxicity of compounds **8a–c** and **13a–c** containing a *p*-chlorophenyl group[a]

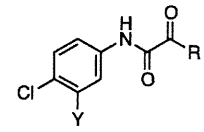

Compd	R	Y	IC_{50}[b] (μM) YTA48P	CC_{50}[c] (μM)
1	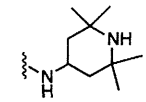	H	0.61	110
8a	**A**	F	0.32	94
8b	**A**	Cl	4.1	36
8c	**A**	Me	3.3	38
3	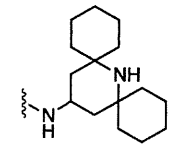	H	0.43	120
13a	**B**	F	0.23	11
13b	**B**	Cl	0.62	11
13c	**B**	Me	2.6	15

[a] All data are the mean values from three of more independent experiments.
[b] IC_{50} values of the multi-round assay are based on the inhibition of HIV-1-induced cytopathogenicity in PM1/CCR5 cells.
[c] CC_{50} values are based on the reduction of the viability of mock-infected PM1/CCR5 cells.

Table 2
Anti-HIV activity and cytotoxicity of compounds **9a–c** and **14a–c** containing a *p*-tolyl group[a]

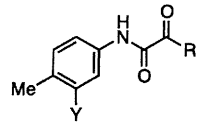

Compd	R	Y	IC_{50}[b] (μM) YTA48P	CC_{50}[c] (μM)
2	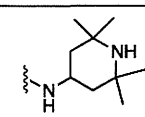	H	9.0	260
9a	**A**	F	2.8	110
9b	**A**	Cl	3.2	62
9c	**A**	Br	>10	32
14a	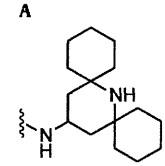	F	0.54	91
14b	**B**	Cl	6.2	11
14c	**B**	Br	3.2	11

[a] All data are the mean values from three of more independent experiments.
[b] IC_{50} values of the multi-round assay are based on the inhibition of HIV-1-induced cytopathogenicity in PM1/CCR5 cells.
[c] CC_{50} values are based on the reduction of the viability of mock-infected PM1/CCR5 cells.

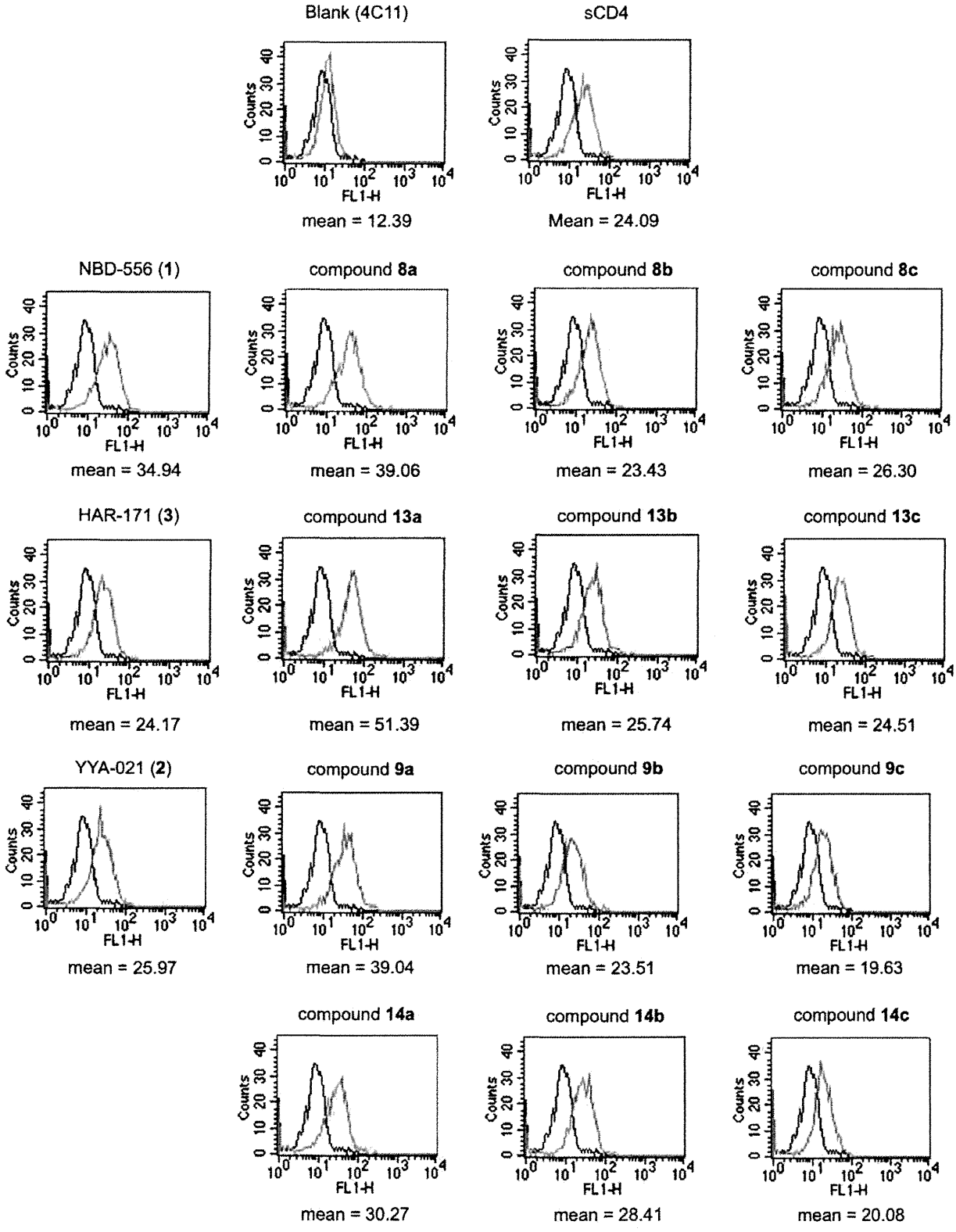

Figure 4. FACS analysis of synthetic compounds **8**, **9**, **13** and **14**.

approximately 10-fold lower than that of compound **8a**. The cytotoxicity of **8b** and **8c** is relatively stronger than that of **8a** (CC_{50} of **8b** = 36 μM and CC_{50} of **8c** = 38 μM). Compounds **13a–c** with hydrophobic cyclohexyl groups in the piperidine moiety showed more potent anti-HIV activity than the corresponding compounds **8a–c**, confirming the contribution of the bulky hydrophobic group(s) to an increase of antiviral activity. Our lead compound **3** showed significant anti-HIV activity comparable to that of compound **8a** (IC_{50} = 0.43 μM) but, consistent with previous results, exhibited lower cytotoxicity. In particular, compound **13a** with a *m*-fluoro-*p*-chlorophenyl group exhibited the highest anti-HIV activity. The IC_{50} value of **13a** was 0.23 μM, whose potency was

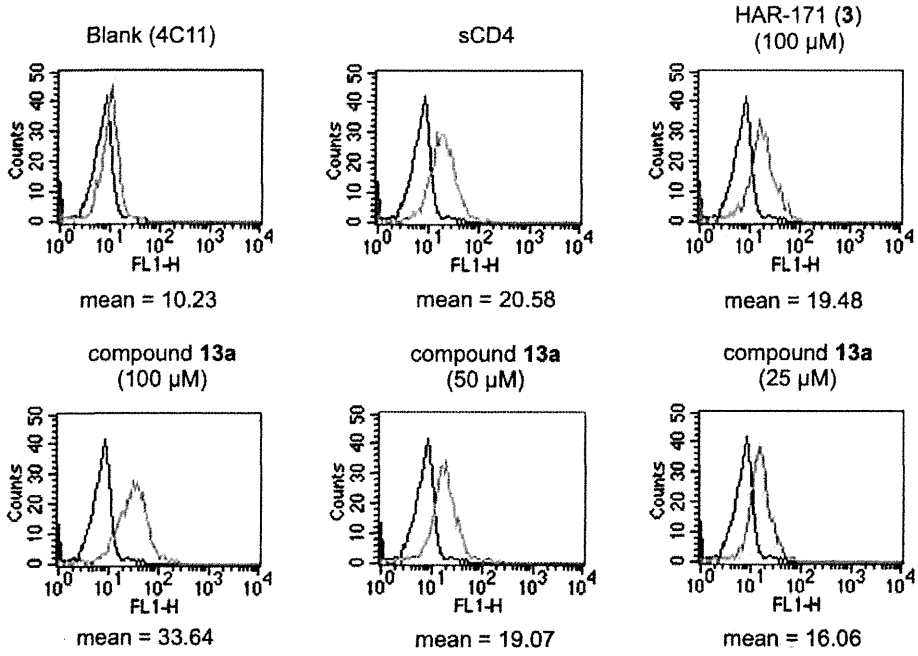

Figure 5. FACS analysis of **3** and **13a** in different concentrations.

approximately twice as high as that of compound **3**. Notably, compound **13b** with a *m,p*-dichlorophenyl group showed 7-fold more potent anti-HIV activity than the corresponding compound **8b**. Compound **13c**, which has a *p*-chloro-*m*-tolyl group, showed potent anti-HIV activity comparable to that of the corresponding compound **8c** and an increase of cytotoxicity (CC_{50} = 15 μM). We observed a tendency for compounds **13a–c** with both hydrophobic cyclohexyl groups and a *m,p*-disubstituted phenyl group to exhibit higher cytotoxicity than the corresponding tetramethyl-type compounds **8a–c**. No clear reason for an increase of cytotoxicity in the *m,p*-disubstituted phenyl group-containing compounds is apparent.

Assay results for the compounds **9a–c** and **14a–c** with a *p*-tolyl group are shown in Table 2. As expected, replacement of the *p*-chloro substituent with a *p*-methyl group resulted in somewhat reduction of anti-HIV activity. Compound **2**, YYA-021 has significant anti-HIV activity (IC_{50} = 9.0 μM) and exhibits the lowest cytotoxicity among all of the compounds tested (CC_{50} = 260 μM). These results are consistent with our previous SAR studies involving the aromatic ring. Introduction of a fluorine at the *meta*-position of the *p*-tolyl group, e.g. in compound **9a** and **14a**, improved the antiviral activity, as observed with **8a** and **13a** and a similar tendency was observed for compound **9b** with a *m*-chloro-*p*-tolyl group. In particular, compound **14a** with cyclohexyl groups and a *m*-fluoro-*p*-tolyl group showed slightly higher anti-HIV activity than the parent compound **1**. Among the compounds with *m*-bromo-*p*-tolyl groups, it was found that compound **9c**, with a 2,2,6,6-tetramethylpiperidine group, showed no anti-HIV activity at a concentration below 10 μM, whereas compound **14c** with hydrophobic cyclohexyl groups attached to the piperidine moiety, showed moderate activity (IC_{50} = 3.2 μM), indicating that the hydrophobic modification of piperidine ring can contribute to an increase in anti-HIV activity.

All the synthetic compounds were evaluated for their CD4 mimicry on the conformational changes in gp120 by fluorescence activated cell sorting (FACS) analysis, and the results are shown in Figure 4. The profile of binding of a CD4-induced (CD4i) monoclonal antibody (4C11) to the Env-expressing cell surface pretreated with the synthetic compounds was assessed in terms of the mean fluorescence intensity (MFI). The increase in binding affinity for 4C11 (by the pretreatment with synthetic compounds) suggests that those compounds can reflect the CD4 mimicry as a consequence of the conformational changes in gp120. Our previous studies disclosed that the profiles of the binding to the cell surface pretreated with **1**, **2**, or **3** were similar to those observed in pretreatment with soluble CD4, indicating that these compounds offer a significant enhancement of binding affinity for 4C11.[8] As shown in Figure 4, similar results were obtained with those compounds in this FACS analysis (MFI of **1**, **2**, and **3** = 34.94, 25.97, and 24.17, respectively). A notable increase in binding affinity for 4C11 was observed in essentially all the synthetic compounds. The compounds **8a**, **9a**, **13a** and **14a** with a *meta*-fluorine in the aromatic ring, showed significant anti-HIV activity, and produced a substantial increase in binding affinity for 4C11. These results suggested that the introduction of a fluorine group at the meta position of the aromatic ring is significant not only for the increase of anti-HIV activity, but also for the enhancement of a CD4 mimicry. In particular, a remarkable improvement in binding affinity for 4C11 was observed with **13a** (MFI = 51.39) which has twofold more potent anti-HIV activity than the lead compound **3** (HAR-171), and is the most active compound in terms of both anti-HIV activity and the CD4 mimicry resulting from the conformational change in gp120. The profiles of pretreatment of the cell surface with compounds **8b** and **13b** having a *m,p*-dichlorophenyl group, compounds **8c** and **13c** having a *p*-chloro-*m*-tolyl group, and compounds **9b** and **14b** with a *m*-chloro-*p*-tolyl group were similar to results obtained for **3**, suggesting that these compounds produced slightly lower enhancement compared to those of compounds **8a**, **9a**, **13a** and **14a** but significant levels of binding affinity for 4C11. On the other hand, pretreatment with compounds **9c**, which failed to show significant anti-HIV activity and **14c**, which had moderate anti-HIV activity resulted in a slight decrease of binding affinity for 4C11, suggesting that the introduction of a Br group at the *meta*-position of *p*-tolyl group is not advantageous to a CD4 mimicry, possibly due to the steric hindrance caused by the two bulky substituents. These results are consistent with previous observations that a limited size and electron-withdrawing ability of the aromatic substituents are required for potent anti-HIV activity and CD4 mimicry.[8a]

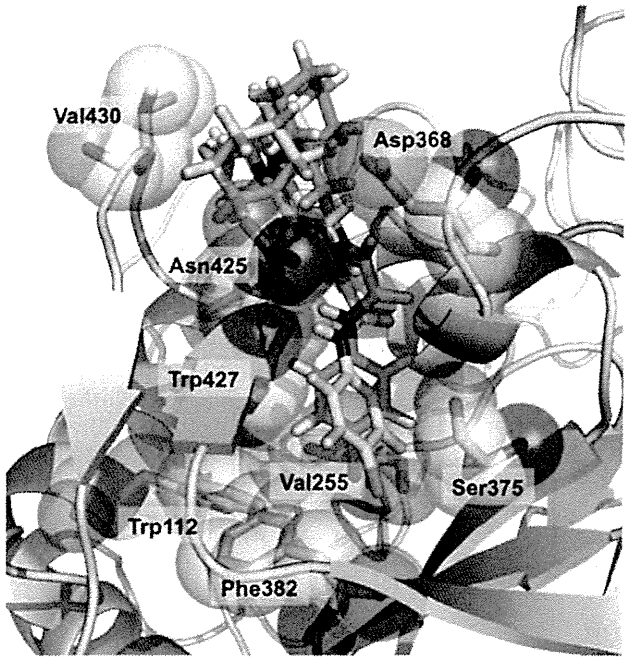

Figure 6. The modeled structure of **13a** (yellow carbon atoms) in the complex with the Phe43 cavity in gp120 (3TGS) overlaid with the modeled structure of **3** (green carbon atoms).

Since **13a** showed higher CD4 mimicry than the other compounds tested, the effect of the solution concentration of **13a** on the binding affinity for 4C11 was investigated. As shown in Figure 5, pretreatment of the cell surface with a 100 μM solution of **13a** produced a higher increase in the binding affinity for 4C11 than pretreatment with the same concentration of compound **3**. Interestingly, the profile pretreated with a 50 μM solution of **13a** was similar to that with a 100 μM of compound **3**, and even with a 25 μM solution of **13a** a potent enhancement of the binding affinity for 4C11 was observed: MFI of **13a** at concentrations of 50 μM and 25 μM = 19.07 and 16.06, respectively. This observation suggests that **13a** could serve as a novel lead compound for the development of envelope protein openers for the use combined with neutralizing antibodies because of its effectiveness at low concentrations.

The substantial increase in the CD4 mimicry of **13a** even at a low concentration is not easily explained because HAR-171 (**3**) and **13a** would be expected to form the similar binding modes with gp120. A probable contribution of **13a** is suggested by modeling studies docked into the Phe43 cavity in gp120 (3TGS) in which the depth and direction of the aromatic ring of **13a** is slightly different from those in compound **3** (Fig. 6), leading to the possible formation of appropriate interactions with the hydrophobic amino acid residues such as Val255 and Phe382, and therefore explaining the increased potency observed in the anti-HIV activity and CD4 mimicry of **13a**.

3. Conclusion

CD4 mimics are attractive agents not only for the development of a novel class of HIV entry inhibitors but also as possible cooperating agents for the neutralizing antibodies—that is, envelope protein openers. In the present study, a structure–activity relationship study of a series of CD4 mimic compounds was performed with a view to improving the biological activity of HAR-171 (**3**), which was identified in our previous studies as a promising lead compound with anti-HIV activity, cytotoxicity and CD4 mimicry resulting from the conformational change in gp120. Systematic modification of the *meta*- and *para*-substituents of the aromatic ring of **3** led to some potent compounds. In particular, **13a**, which has a bulky hydrophobic group on its piperidine ring and a *m*-fluoro-*p*-chlorophenyl group, demonstrated twofold more potent anti-HIV activity and much higher CD4 mimicry than **2** following the conformational changes in gp120, although the cytotoxicity of **13a** is relatively high. Further structural modification studies of the aromatic ring and the oxalamide linker to improve pharmaceutical profiles will be the subject of future reports.

4. Experimentals

^{1}H NMR and ^{13}C NMR spectra were recorded using a Bruker Avance III spectrometer. Chemical shifts are reported in δ (ppm) relative to Me_4Si (in $CDCl_3$) as internal standard. Low- and high-resolution mass spectra were recorded on a Bruker Daltonics microTOF focus in the positive and negative detection mode. For flash chromatography, silica gel 60 N (Kanto Chemical Co., Inc.) was employed. Microwave reactions were performed in Biotage Microwave Reaction Kit (sealed vials) in an Initiator™ (Biotage). The wattage was automatically adjusted to maintain the desired temperature for the desired period of time.

4.1. Chemistry

4.1.1. Ethyl 2-((4-chloro-3-fluorophenyl)amino)-2-oxoacetate (6a)

To a stirred solution of 3-fluoroaniline (1.11 g, 10.0 mmol) in $CHCl_3$ (30.0 mL) was added dropwise *N*-chlorosuccinimide (NCS) in $CHCl_3$ (20.0 mL) at 0 °C. The mixture was stirred at 0 °C for 42 h. After the reaction mixture was concentrated under reduced pressure, the residue was dissolved in Et_2O. The mixture was washed with water, and dried over $MgSO_4$. Concentration under reduced pressure followed by flash chromatography over silica gel with EtOAc/*n*-hexane gave 4-chloro-3-fluoroaniline (259.4 g, 18% yield) as crystalline solids. To a stirred solution of the above aniline (259.4 mg, 1.78 mmol) in THF (8.9 mL) were added at 0 °C ethyl chloroglyoxylate (237.3 μL, 2.14 mmol) and Et_3N (296.6 μL, 2.14 mmol). The mixture was stirred at room temperature for 12 h. After the precipitate was filtrated off, the filtrate solution was concentrated under reduced pressure. The residue was dissolved in EtOAc, and washed with 1.0 M HCl, saturated $NaHCO_3$ and brine, then dried over $MgSO_4$. Concentration under reduced pressure to provide the title compound **6a** (435.2 mg, 99% yield) as brown crystals, which was used without further purification.

^{1}H NMR (500 MHz, $CDCl_3$) δ 1.44 (t, J = 7.50 Hz, 3H), 4.43 (q, J = 7.50 Hz, 2H), 7.24–7.25 (m, 1H), 7.35–7.40 (m, 1H), 7.70–7.75 (m, 1H), 8.93 (br, 1H); ^{13}C NMR (125 MHz, $CDCl_3$) δ 13.0, 64.1, 108.5 (d, J = 26.3 Hz), 115.9 (d, J = 3.75 Hz), 117.3 (d, J = 18.8 Hz), 130.9 (d, J = 10.0 Hz), 135.9, 153.9, 158.1 (d, J = 246.3 Hz), 160.5; HRMS (ESI), m/z calcd for $C_{10}H_{10}ClFNO_3$ (MH^-) 244.0182, found 244.0183.

4.1.2. Ethyl 2-((3,4-dichlorophenyl)amino)-2-oxoacetate (6b)

To a stirred solution of 3,4-dichloroaniline **4b** (1.94 g, 12.0 mmol) in THF (20.0 mL) were added ethyl chloroglyoxylate (1.11 mL, 10.0 mmol) and Et_3N (15.2 mL, 11.0 mmol) at 0 °C. The mixture was stirred at room temperature for 6 h. After the precipitate was filtrated off, the filtrate solution was concentrated under reduced pressure. The residue was dissolved in EtOAc, and washed with 1.0 M HCl, saturated $NaHCO_3$ and brine, then dried over $MgSO_4$. Concentration under reduced pressure to provide the title compound **6b** (1.58 g, 95% yield) as white powder, which was used without further purification.

^{1}H NMR (500 MHz, $CDCl_3$) δ 1.44 (t, J = 7.00 Hz, 3H), 4.43 (q, J = 7.00 Hz, 2H), 7.44 (d, J = 8.50 Hz, 1H), 7.49–7.51 (m, 1H), 7.87, 2.35 (d, J = 2.50 Hz, 1H); ^{13}C NMR (125 MHz, $CDCl_3$) δ 14.0, 64.0, 119.0, 121.5, 129.0, 130.8, 133.2, 135.7, 153.9, 160.5; HRMS (ESI), m/z calcd for $C_{10}H_{10}Cl_2NO_3$ (MH^+) 262.0038, found 262.0031.

4.1.3. Ethyl 2-((4-chloro-3-methylphenyl)amino)-2-oxoacetate (6c)

By use of a procedure similar to that described for the preparation of compound **6b**, the aniline **4c** (3.34 g, 24.0 mmol) was converted into the title compound **6c** (4.63 g, 96% yield) as white powder.

^{1}H NMR (500 MHz, $CDCl_3$) δ 1.43 (t, J = 7.00 Hz, 3H), 2.38 (s, 3H), 4.42 (q, J = 7.00 Hz, 2H), 7.33 (d, J = 8.50 Hz, 1H), 7.43–7.46 (m, 1H), 7.51–7.54 (m, 1H), 8.82 (s, 1H); ^{13}C NMR (125 MHz, $CDCl_3$) δ 14.0, 20.2, 63.8, 118.5, 122.0, 129.7, 130.9, 134.8, 137.1, 153.8, 160.9; HRMS (ESI), m/z calcd for $C_{11}H_{13}ClNO_3$ (MH^+) 242.0578, found 242.0568.

4.1.4. Ethyl 2-((3-fluoro-4-methylphenyl)amino)-2-oxoacetate (7a)

By use of a procedure similar to that described for the preparation of compound **6b**, the aniline **5a** (3.00 g, 24.0 mmol) was converted into the title compound **7a** (4.24 g, 94% yield) as white powder.

^{1}H NMR (500 MHz, $CDCl_3$) δ 1.43 (t, J = 7.20 Hz, 3H), 2.25 (s, 3H), 4.42 (q, J = 6.80 Hz, 2H), 7.12–7.21 (m, 2H), 7.48–7.56 (m, 1H), 8.83 (s, 1H); ^{13}C NMR (125 MHz, $CDCl_3$) δ 14.2 (2C), 63.8, 107.1 (d, J = 27.5 Hz), 115.0 (d, J = 10.0 Hz), 122.3 (d, J = 17.5 Hz), 131.6 (d, J = 6.25 Hz), 135.3 (d, J = 13.8 Hz), 153.8, 160.8, 161.1 (d, J = 243.8 Hz); HRMS (ESI), m/z calcd for $C_{11}H_{13}FNO_3$ (MH^+) 226.0879, found 226.0878.

4.1.5. Ethyl 2-((3-chloro-4-methylphenyl)amino)-2-oxoacetate (7b)

By use of a procedure similar to that described for the preparation of compound **6b**, the aniline **5b** (3.40 g, 24.0 mmol) was converted into the title compound **7b** (5.19 g, 94% yield) as white powder.

^{1}H NMR (500 MHz, $CDCl_3$) δ 1.43 (t, J = 7.00 Hz, 3H), 2.35 (s, 3H), 4.42 (q, J = 7.00 Hz, 2H), 7.22 (d, J = 8.50 Hz, 1H), 7.41–7.43 (m, 1H), 7.71 (d, J = 2.00 Hz, 1H), 8.83 (s, 1H); ^{13}C NMR (125 MHz, $CDCl_3$) δ 14.0, 20.0, 63.8, 118.0, 120.3, 131.2, 133.3, 134.7, 135.0, 153.8, 160.8; HRMS (ESI), m/z calcd for $C_{11}H_{13}ClNO_3$ (MH^+) 242.0584, found 242.0573.

4.1.6. Ethyl 2-((3-bromo-4-methylphenyl)amino)-2-oxoacetate (7c)

By use of a procedure similar to that described for the preparation of compound **6b**, the aniline **5c** (4.47 g, 27.0 mmol) was converted into the title compound **7c** (6.24 g, 96% yield) as white powder.

^{1}H NMR (500 MHz, $CDCl_3$) δ 1.43 (t, J = 7.00 Hz, 3H), 2.38 (s, 3H), 4.42 (q, J = 7.00 Hz, 2H), 7.23 (t, J = 8.50 Hz, 1H), 7.48–7.53 (m, 1H), 7.83–7.90 (m, 1H), 8.80 (s, 1H); ^{13}C NMR (125 MHz, $CDCl_3$) δ 14.0, 22.4, 63.9, 118.7, 123.4, 125.0, 131.0, 135.0, 135.2, 153.7, 160.8; HRMS (ESI), m/z calcd for $C_{11}H_{13}BrNO_3$ (MH^+) 286.0079, found 286.0068.

4.1.7. N^1-(4-Chloro-3-fluorophenyl)-N^2-(2,2,6,6-tetramethylpiperidin-4-yl)oxalamide (8a)

To a solution of compound **6a** (70.0 mg, 0.286) in EtOH (2.9 mL) were added Et_3N (0.200 mL, 1.45 mmol) and 2,2,6,6-tetramethylpiperidin-4-amine (0.150 mL, 0.870 mmol). The reaction mixture was stirred for 3 h at 150 °C under microwave irradiation. After being concentrated in vacuo, the residue was extracted with $CHCl_3$, and washed with saturated $NaHCO_3$ and brine, then dried over $MgSO_4$. Concentration under reduced pressure to provide the title compound **8a** (34.6 mg, 34% yield) as white powder.

^{1}H NMR (500 MHz, $CDCl_3$) δ 0.99–1.50 (m, 15H), 1.92 (dd, J = 3.50, 9.00 Hz, 2H), 4.20–4.32 (m, 1H), 7.21–7.25 (m, 1H), 7.34–7.41 (m, 1H), 7.69–7.73 (m 1H), 9.31 (br, 1H); ^{13}C NMR (125 MHz, $CDCl_3$) δ 28.4, 34.8, 43.8, 44.5, 51.0, 108.3 (d, J = 26.3 Hz), 115.8 (d, J = 3.75 Hz), 117.1 (d, J = 17.5 Hz), 130.8, 136.2 (d, J = 8.75 Hz), 157.6, 158.1 (d, J = 247.5 Hz), 158.4; HRMS (ESI), m/z calcd for $C_{17}H_{24}ClFN_3O_2$ (MH^+) 356.1536, found 356.1548.

4.1.8. N^1-(3,4-Dichlorophenyl)-N^2-(2,2,6,6-tetramethylpiperidin-4-yl)oxalamide (8b)

By use of a procedure similar to that described for the preparation of compound **8a**, the compound **6b** (261.0 mg, 1.00 mmol) was converted into the title compound **8b** (520.0 mg, 70% yield) as white powder.

^{1}H NMR (500 MHz, $CDCl_3$) δ 1.07 (t, J = 12.0 Hz, 2H), 1.16 (s, 6H), 1.28 (s, 6H), 1.90–1.93 (m, 2H), 4.20–4.32 (m, 1H), 7.26 (m, 1H), 7.40–7.48 (m, 2H), 7.88 (s, 1H), 9.33 (s, 1H); ^{13}C NMR (125 MHz, $CDCl_3$) δ 28.5 (2C), 34.9 (2C), 43.8, 44.6 (2C), 50.9 (2C), 119.0, 121.4, 128.7, 130.8, 133.1, 135.8, 157.7, 158.5; HRMS (ESI), m/z calcd for $C_{17}H_{22}Cl_2N_3O_2$ (MH^-) 370.1095, found 370.1105.

4.1.9. N^1-(4-Chloro-3-methylphenyl)-N^2-(2,2,6,6-tetramethylpiperidin-4-yl)oxalamide (8c)

By use of a procedure similar to that described for the preparation of compound **8a**, the compound **6c** (482.0 mg, 2.00 mmol) was converted into the title compound **8c** (364.0 mg, 49% yield) as white powder.

^{1}H NMR (500 MHz, $CDCl_3$) δ 1.07 (t, J = 12.0 Hz, 2H), 1.15 (s, 6H), 1.28 (s, 6H), 1.86–1.94 (m, 2H), 4.15–4.31 (m, 1H), 7.21–7.24 (m, 1H), 7.32–7.38 (m, 2H), 7.74 (s, 1H), 9.24 (s, 1H); ^{13}C NMR (125 MHz, $CDCl_3$) δ 19.6, 28.5 (2C), 34.9 (2C), 43.7, 44.7 (2C), 50.9 (2C), 117.9, 120.2, 131.2, 133.1, 134.7, 135.1, 157.5, 158.8; HRMS (ESI), m/z calcd for $C_{18}H_{25}ClN_3O_2$ (MH^-) 350.1641, found 350.1656.

4.1.10. N^1-(3-Fluoro-4-methylphenyl)-N^2-(2,2,6,6-tetramethylpiperidin-4-yl)oxalamide (9a)

By use of a procedure similar to that described for the preparation of compound **8a**, the compound **7a** (225.0 mg, 1.00 mmol) was converted into the title compound **9a** (161.0 mg, 48% yield) as white powder.

^{1}H NMR (500 MHz, $CDCl_3$) δ 1.07 (t, J = 12.5 Hz, 2H), 1.15 (s, 6H), 1.28 (s, 6H), 1.92 (dd, J = 12.5, 3.50 Hz, 2H), 2.26 (s, 3H), 4.12–4.32 (m, 1H), 7.12–7.20 (m, 2H), 7.30–7.37 (m, 1H), 7.48–7.54 (m, 1H), 9.27 (s, 1H); ^{13}C NMR (125 MHz, $CDCl_3$) δ 14.2, 28.5 (2C), 34.9 (2C), 43.7, 44.7 (2C), 50.9 (2C), 107.1 (d, J = 26.3 Hz), 115.0, 121.8 (d, J = 17.5 Hz) 131.6, 135.4, (d, J = 15.0 Hz), 157.5, 158.8, 161.1 (d, J = 242.5 Hz); HRMS (ESI), m/z calcd for $C_{18}H_{25}FN_3O_2$ (MH^-) 334.1936, found 334.1942.

4.1.11. N^1-(3-Chloro-4-methylphenyl)-N^2-(2,2,6,6-tetramethylpiperidin-4-yl)oxalamide (9b)

By use of a procedure similar to that described for the preparation of compound **8a**, the compound **7b** (482.0 mg, 1.00 mmol) was converted into the title compound **9b** (448.0 mg, 48% yield) as white powder.

^{1}H NMR (500 MHz, $CDCl_3$) δ 1.09 (t, J = 12.5 Hz, 3H), 1.18 (s, 6H), 1.30 (s, 6H), 1.93–1.95 (m, 2H), 2.41 (s, 3H), 4.20–4.34 (m, 1H), 7.30–7.37 (m, 2H), 7.44–7.46 (m, 1H), 7.53 (d, J = 2.50 Hz, 1H), 9.25 (s, 1H); ^{13}C NMR (125 MHz, $CDCl_3$) δ 20.3, 28.5 (2C), 34.9 (2C), 43.7, 44.7 (2C), 50.9 (2C), 118.5, 122.0, 130.0, 130.7, 134.8, 137.1, 157.5, 158.8; HRMS (ESI), m/z calcd for $C_{18}H_{25}ClN_3O_2$ (MH^-) 350.1641, found 350.1636.

4.1.12. N^1-(3-Bromo-4-methylphenyl)-N^2-(2,2,6,6-tetramethylpiperidin-4-yl)oxalamide (9c)

By use of a procedure similar to that described for the preparation of compound **8a**, the compound **7c** (285.0 mg, 1.00 mmol) was converted into the title compound **9c** (157.0 mg, 40% yield) as white powder.

^{1}H NMR (500 MHz, $CDCl_3$) δ 1.07 (t, J = 12.5 Hz, 3H), 1.15 (s, 6H), 1.28 (s, 6H), 1.91 (dd, J = 8.00, 4.00 Hz, 2H), 2.38 (s, 3H), 3.70–3.75 (m, 1H), 7.22 (d, J = 8.50 Hz, 1H), 7.30–7.37 (m, 1H), 7.43–7.45 (m, 1H), 7.90 (d, J = 2.50 Hz, 1H), 9.25 (s, 1H); ^{13}C NMR (125 MHz, $CDCl_3$) δ 22.4, 28.5 (2C), 34.9 (2C), 43.7, 44.7 (2C), 50.9 (2C), 118.6, 123.4, 125.0, 131.0, 134.9 (2C), 157.5, 158.8; HRMS (ESI), m/z calcd for $C_{18}H_{25}BrN_3O_2$ (MH^-) 394.1136, found 394.1158.

4.1.13. Amine (12)

The compound **11** was prepared according to the reported procedure.[14] To a stirred solution of piridone **11** (247.8 mg, 1.05 mmol) in MeOH (2.10 mL) was added p-methoxybenzylamine (0.41 mL, 3.15 mmol). After being stirred at room temperature for 23 h, sodium cyanoborohydride was added and stirred at room temperature for 48 h. The reaction mixture was poured into saturated $NaHCO_3$ and extracted with EtOAc, then dried over $MgSO_4$. After concentration under reduced pressure, the residue was treated with 1 M TMS in THF (4.8 mL). The mixture was stirred at 0 °C for 14 h. Concentration under reduced pressure followed by short chromatography with $CHCl_3$/MeOH gave the PMB-protected amine. To a solution of the above amine (584.0 mg, 1.64 mmol) in CH_3CN/H_2O (13.1 mL, v:v = 2:1) was added CAN (2.74 g, 8.2 mmol). The mixture was stirred at room temperature for 14 h. The reaction mixture was diluted with 0.5 M HCl and washed with CH_2Cl_2. The water layer was alkalized and extracted with EtOAc, then dried over Na_2SO_4. Concentration under reduced pressure followed by flash chromatography over silica gel with EtOAc–EtOH (4:1) to gave the title compound **12** (175.5 mg, 71% yield) as a yellow oil.

^{1}H NMR (500 MHz, $CDCl_3$) δ 1.15–1.85 (m, 24H), 2.95–3.05 (m, 1H); ^{13}C NMR (125 MHz, $CDCl_3$) δ 22.2 (2C), 22.8 (2C), 26.2 (2C), 37.3 (2C), 42.3 (2C), 43.6 (2C), 47.0, 53.2 (2C); HRMS (ESI), m/z calcd for $C_{15}H_{29}N_2$ (MH^+) 237.2325, found 237.2321.

4.1.14. N^1-((4-Chloro-3-fluorophenyl)-N^2-(2,6-dicyclohexylpiperidin-4-yl)oxalamide (13a)

By use of a procedure similar to that described for the preparation of compound **8a**, the compound **6a** (36.8 mg, 0.150 mmol) was converted into the title compound **13a** (7.6 mg, 12% yield) as yellow powder.

^{1}H NMR (400 MHz, $CDCl_3$) δ 0.71–2.28 (m, 24H), 2.03–2.20 (m, 2H), 4.02–4.16 (m, 1H), 7.13–7.18 (m, 1H), 7.27–7.33 (m, 1H), 7.62–7.66 (m, 1H), 9.25 (br, 1H); ^{13}C NMR (125 MHz, $CDCl_3$) δ 14.1, 22.0 (2C), 22.6 (2C), 25.8 (2C), 29.3, 29.7 (2C), 31.9, 70.5, 108.3 (d, J = 26.3 Hz), 115.8, 117.1 (d, J = 18.8 Hz), 130.8, 136.2 (d, J = 10.0 Hz), 157.6, 158.1 (d, J = 247.5 Hz), 158.6; HRMS (ESI), m/z calcd for $C_{23}H_{32}ClFN_3O_2$ (MH^+) 436.2162, found 436.2156.

4.1.15. N^1-(4-Chlorophenyl)-N^2-(2,6-dicyclohexylpiperidin-4-yl)oxalamide (13b)

By use of a procedure similar to that described for the preparation of compound **8a**, the compound **6b** (31.3 mg, 0.120 mmol) was converted into the title compound **13b** (28.0 mg, 52% yield) as white powder.

^{1}H NMR (400 MHz, $CDCl_3$) δ 0.96 (t, J = 12.5 Hz, 2H), 1.10–1.84 (br, 20H), 2.05–2.19 (m, 2H), 4.08–4.21 (m, 1H), 7.23–7.33 (br, 1H), 7.39–7.46 (m, 2H), 7.88 (t, J = 1.00 Hz, 1H), 9.34 (s, 1H); ^{13}C NMR (125 MHz, $CDCl_3$) δ 14.1, 22.1 (2C), 22.7 (2C), 26.1 (2C), 31.6, 37.2 (2C), 42.6, 43.0, 43.6, 52.6 (2C), 119.0, 121.4, 128.7, 130.8, 133.1, 135.8, 157.7, 158.5; HRMS (ESI), m/z calcd for $C_{23}H_{32}Cl_2N_3O_2$ (MH^+) 452.1872, found 452.1865.

4.1.16. N^1-((4-Chloro-3-methylphenyl)-N^2-(2,6-dicyclohexylpiperidin-4-yl)oxalamide (13c)

By use of a procedure similar to that described for the preparation of compound **8a**, the compound **6c** (121.0 mg, 0.500 mmol) was converted into the title compound **13c** (15.1 mg, 7% yield) as white powder.

^{1}H NMR (500 MHz, $CDCl_3$) δ 0.87–1.88 (br, 22H), 2.09–2.20 (m, 2H), 2.38 (s, 3H), 4.09–4.22 (m, 1H), 7.32–7.33 (m, 1H), 7.41–7.43 (m, 1H), 7.51 (d, J = 2.00 Hz, 1H), 7.73 (m, 1H), 9.24 (s, 1H); ^{13}C NMR (125 MHz, $CDCl_3$) δ 20.2, 22.1 (2C), 22.7 (2C), 26.0 (2C), 29.7, 37.0, 42.3 (2C), 42.8 (2C), 43.4, 52.9 (2C), 118.4, 122.0, 130.0, 130.6, 134.8, 137.1, 157.5, 158.9; HRMS (ESI), m/z calcd for $C_{24}H_{35}ClN_3O_2$ (MH^+) 430.2267, found 430.2264.

4.1.17. N^1-(3-Fluoro-4-methylphenyl)-N^2-(2,6-dicyclohexylpiperidin-4-yl)oxalamide (14a)

By use of a procedure similar to that described for the preparation of compound **8a**, the compound **7a** (225.0 mg, 1.00 mmol) was converted into the title compound **14a** (27.5 mg, 7% yield) as white powder.

^{1}H NMR (500 MHz, $CDCl_3$) δ 0.971 (t, J = 12.5 Hz, 2H), 1.18–1.86 (m, 20H), 2.13–2.16 (m, 2H), 2.26 (s, 3H), 4.09–4.21 (m, 1H), 7.13–7.18 (m, 2H), 7.33 (d, J = 8.00 Hz, 1H), 7.50–7.53 (m, 1H), 9.27 (s, 1H); ^{13}C NMR (125 MHz, $CDCl_3$) δ 14.2, 22.2 (2C), 22.8 (2C), 26.1 (2C), 37.2 (2C), 42.2 (2C), 43.3 (2C), 43.5, 52.6 (m, 2C), 107.0 (d, J = 27.5 Hz), 115.0 (d, J = 3.75 Hz), 121.8 (d, J = 17.5 Hz), 131.6 (d, J = 6.25 Hz), 135.4 (d, J = 10.0 Hz), 157.5, 158.9, 161.3 (d, J = 242.5 Hz); HRMS (ESI), m/z calcd for $C_{24}H_{33}FN_3O_2$ (MH^-) 414.2554, found 414.2562.

4.1.18. N^1-(3-Chloro-4-methylphenyl)-N^2-(2,6-dicyclohexylpiperidin-4-yl)oxalamide (14b)

By use of a procedure similar to that described for the preparation of compound **8a**, the compound **7b** (120.5 mg, 0.500 mmol) was converted into the title compound **14b** (12.9 mg, 6% yield) as white powder.

^{1}H NMR (500 MHz, $CDCl_3$) δ 0.973 (t, J = 12.5 Hz, 2H), 1.18–1.86 (br, 20H), 2.11–2.19 (m, 2H), 2.35 (s, 3H), 4.09–4.21 (m, 1H), 7.20–7.22 (m, 1H), 7.30–7.32 (m, 1H), 7.35–7.37 (d, J = 2.50 Hz, 1H), 7.73 (m, 1H), 9.22 (s, 1H); ^{13}C NMR (125 MHz, $CDCl_3$) δ 19.6, 22.1 (2C), 22.7 (2C), 26.0 (2C), 29.7, 37.0, 42.1 (2C), 42.7 (2C), 43.2, 53.3 (2C), 118.0, 120.3, 131.2, 133.0, 134.7, 135.1, 157.5, 158.8; HRMS (ESI), m/z calcd for $C_{24}H_{33}ClN_3O_2$ (MH^+) 430.2267, found 430.2257.

4.1.19. N^1-(3-Bromo-4-methylphenyl)-N^2-(2,6-dicyclohexylpiperidin-4-yl)oxalamide (14c)

By use of a procedure similar to that described for the preparation of compound **8a**, the compound **7c** (142.0 mg, 0.500 mmol) was converted into the title compound **14c** (11.5 mg, 5% yield) as white powder.

^{1}H NMR (500 MHz, $CDCl_3$) δ 0.67–2.07 (br, 22H), 2.28 (br, 2H), 2.38 (s, 3H), 4.09–4.21 (m, 1H), 7.22 (d, J = 8.00 Hz, 1H), 7.28–7.38 (br, 1H), 7.43 (dd, J = 4.50, 2.50 Hz, 1H), 7.90 (d, J = 2.50 Hz, 1H), 9.21 (s, 1H); ^{13}C NMR (125 MHz, $CDCl_3$) δ 14.1, 22.1 (2C), 22.4 (2C), 22.7 (2C), 25.9, 30.0, 31.6, 36.9 (2C), 42.7 (3C), 52.7, 52.9, 118.6, 123.4, 125.0, 131.0, 134.9, 135.1, 157.4, 158.8; HRMS (ESI), m/z calcd for $C_{24}H_{33}BrN_3O_2$ (MH^+) 474.1762, found 474.1746.

4.2. Antiviral assay and cytotoxicity assay

Anti-HIV activity and cytotoxicity measurements in PM1/CCR5 cells (Yoshimura et al., 2010) were based on viability of cells that

had been infected or not infected with 100 TCID50 of an R5 primary isolate YTA48P exposed to various concentrations of the test compound. After the PM1/CCR5 cells were incubated at 37 °C for 7 days. The 50% inhibitory concentration (IC_{50}) values and the 50% cytotoxic concentration (CC_{50}) were then determined using the Cell Counting Kit-8 assay (Dojindo Laboratories). All assays were performed in duplicate or triplicate.

4.3. FACS analysis

JR-FL (R5, Sub B) chronically infected PM1 cells were pre-incubated with 0.5 μg/mL of sCD4 or 100 μM of a CD4 mimic for 15 min, and then incubated with an anti-HIV-1 mAb, 4C11, at 4 °C for 15 min. The cells were washed with PBS, and fluorescein isothiocyanate (FITC)-conjugated mouse anti-human IgG antibody was used for antibody-staining. Flow cytometry data for the binding of 4C11 (green lines) to the Env-expressing cell surface in the presence of a CD4 mimic are shown among gated PM1 cells along with a control antibody (anti-human CD19: black lines). Data are representative of the results from a minimum of two independent experiments. The number at the bottom of each graph shows the mean fluorescence intensity (MFI) of the antibody 4C11.

4.4. Molecular modeling

Dockings of compounds **3** and **13a** were performed using Molecular Operating Environment modeling package (MOE 2008. 10, Canada), into the crystal structure of gp120 (PDB, entry 3TGS).

Acknowledgements

This work was supported in part by Grant-in-Aid for Scientific Research from the Ministry of Education, Culture, Sports, Science, and Technology of Japan, and Health and Labour Sciences Research Grants from Japanese Ministry of Health, Labor, and Welfare. We are grateful to Professor Yoshio Hayashi and Dr. Fumika Yakushiji, Tokyo University of Pharmacy and Life Sciences for their assistance in the molecular modelings.

Supplementary data

Supplementary data (NMR charts of compounds) associated with this article can be found, in the online version, at http://dx.doi.org/10.1016/j.bmc.2013.02.041.

References and notes

1. Chan, D. C.; Kim, P. S. *Cell* **1998**, *93*, 681.
2. (a) Kadow, J.; Wang, H.-G.; Lin, P.-F. *Curr. Opin. Investig. Dugs* **2006**, *7*, 721; (b) Repik, A.; Clapham, P. R. *Structure* **2008**, *16*, 1603.
3. Holz-Smith, S.; Sun, I. C.; Jin, L.; Matthews, T. J.; Lee, K. H.; Chen, C. H. *Antimicrob. Agents Chemother.* **2001**, *45*, 60.
4. Lin, P.-F.; Blair, W.; Wang, T.; Spicer, T.; Guo, Q.; Zhou, N.; Gong, Y.-F.; Wang, H.-F. H.; Rose, R.; Yamanaka, G.; Robinson, B.; Li, C.-B.; Fridell, R.; Deminie, C.; Demers, G.; Yang, Z.; Zadjura, L.; Meanwell, N.; Colonno, R. *Proc. Natl. Acad. Sci. U.S.A.* **2003**, *100*, 11013.
5. Zhao, Q.; Ma, L.; Jiang, S.; Lu, H.; Liu, S.; He, Y.; Strick, N.; Neamati, N.; Debnath, A. K. *Virology* **2005**, *339*, 213.
6. (a) Madani, N.; Schön, A.; Princiotto, A. M.; LaLonde, J. M.; Courter, J. R.; Soeta, T.; Ng, D.; Wang, L.; Brower, E. T.; Xiang, S.-H.; Do Kwon, Y.; Huang, C.-C.; Wyatt, R.; Kwong, P. D.; Freire, E.; Smith, A. B., III; Sodroski, J. *Structure* **2008**, *16*, 1689; (b) LaLonde, J. M.; Elban, M. A.; Courter, J. R.; Sugawara, A.; Soeta, T.; Madani, N.; Princiotto, A. M.; Kwon, Y. D.; Kwong, P. D.; Schön, A.; Freire, E.; Sodroski, J.; Smith, A. B., III *Bioorg. Med. Chem. Lett.* **2011**, *20*, 354; (c) LaLonde, J. M.; Kwon, Y. D.; Jones, D. M.; Sun, A. W.; Courter, J. R.; Soeta, T.; Kobayashi, T.; Princiotto, A. M.; Wu, X.; Schön, A.; Freire, E.; Kwong, P. D.; Mascola, J. R.; Sodroski, J.; Madani, N.; Smith, A. B., III *J. Med. Chem.* **2012**, *55*, 4382.
7. Curreli, F.; Choudhury, S.; Pyatkin, I.; Zagorodnikov, V. P.; Bulay, A. K.; Altieri, A.; Kwon, Y. D.; Kwon, P. D.; Debnath, A. K. *J. Med. Chem.* **2012**, *55*, 4764.
8. (a) Yamada, Y.; Ochiai, C.; Yoshimura, K.; Tanaka, T.; Ohashi, N.; Narumi, T.; Nomura, W.; Harada, S.; Matsushita, S.; Tamamura, H. *Bioorg. Med. Chem. Lett.* **2010**, *20*, 354; (b) Narumi, T.; Ochiai, C.; Yoshimura, K.; Harada, S.; Tanaka, T.; Nomura, W.; Arai, H.; Ozaki, T.; Ohashi, N.; Matsushita, S.; Tamamura, H. *Bioorg. Med. Chem. Lett.* **2010**, *20*, 5853; (c) Narumi, T.; Arai, H.; Yoshimura, K.; Harada, S.; Nomura, W.; Matsushita, S.; Tamamura, H. *Bioorg. Med. Chem.* **2011**, *19*, 6735.
9. (a) Schön, A.; Madani, N.; Klein, J. C.; Hubicki, A.; Ng, D.; Yang, X.; Smith, A. B., III; Sodroski, J.; Freire, E. *Biochemistry* **2006**, *45*, 10973; (b) Schön, A.; Lam, S. Y.; Freire, E. *Future Med. Chem.* **2011**, *3*, 1129.
10. Yoshimura, K.; Harada, S.; Shibata, J.; Hatada, M.; Yamada, Y.; Ochiai, C.; Tamamura, H.; Matsushita, S. *J. Virol.* **2010**, *84*, 7558.
11. Kwon, Y. D.; Finzi, A.; Wu, X.; Dogo-Isonagie, C.; Lee, L. K.; Moore, L. R.; Schmidt, S. D.; Stuckey, J.; Yang, Y.; Zhou, T.; Zhu, J.; Vicic, D. A.; Debnath, A. K.; Shapiro, L.; Bewley, C. A.; Mascola, J. R.; Sodroski, J. G.; Kwong, P. D. *Proc. Natl. Acad. Sci. U.S.A.* **2012**, *109*, 5663.
12. (a) Kwong, P. D.; Wyatt, R.; Robinson, J.; Sweet, R. W.; Sodroski, J.; Hendrickson, W. A. *Nature* **1998**, *393*, 648; (b) Kwong, P. D.; Wyatt, R.; Mcajeed, S.; Robinson, J.; Sweet, R. W.; Sodroski, J.; Hendrickson, W. A. *Structure* **2000**, *8*, 1329.
13. McFarland, C.; Vicic, D. A.; Debnath, A. K. *Synthesis* **2006**, 807.
14. Sakai, K.; Yamada, K.; Yamasaki, T.; Kinoshita, Y.; Mito, F.; Utsumi, H. *Tetrahedron* **2010**, *66*, 2311.

Virology 423 (2012) 107–118

Contents lists available at SciVerse ScienceDirect

Virology

journal homepage: www.elsevier.com/locate/yviro

Lymph nodes harbor viral reservoirs that cause rebound of plasma viremia in SIV-infected macaques upon cessation of combined antiretroviral therapy

Mariko Horiike [a], Shingo Iwami [a,b,c], Makoto Kodama [d], Akihiko Sato [d], Yuji Watanabe [a], Mika Yasui [a], Yuki Ishida [a], Takeshi Kobayashi [a], Tomoyuki Miura [a], Tatsuhiko Igarashi [a,*]

[a] Laboratory of Primate Model, Experimental Research Center for Infectious Diseases, Institute for Virus Research, Kyoto University, Kyoto 606-8507, Japan
[b] Precursory Research for Embryonic Science and Technology (PRESTO), Japan Science and Technology Agency (JST), Kawaguchi, Saitama 332-0012, Japan
[c] Graduate School of Mathematical Sciences, The University of Tokyo, Meguro-ku, Tokyo 153-8914, Japan
[d] Medical Research Laboratories, Shionogi & Co. Ltd., Osaka 566-0022, Japan

ARTICLE INFO

Article history:
Received 27 September 2011
Returned to author for revision
6 November 2011
Accepted 29 November 2011
Available online 21 December 2011

Keywords:
SIV
Antiretroviral therapy
HIV-1
HAART
Rebound of plasma viremia
Reservoirs
Animal model

ABSTRACT

Attempts to find a cure for HIV infection are hindered by the presence of viral reservoirs that resist highly active antiretroviral therapy. To identify the properties of these reservoirs, four SIV239-infected Rhesus macaques were treated with combined antiretroviral therapy (cART) for 1 year. While plasma viral RNA (vRNA) was effectively suppressed, a systemic analysis revealed that vRNA was distributed in the following order: lymphatic tissues > lungs and intestine > other tissues. Histochemistry yielded no cells with viral signals. To increase the chance of detection, two additional SIV-infected animals were treated and analyzed on Day 10 after the cessation of cART. These animals exhibited similar vRNA distribution patterns to the former animals, and immunohistochemistry revealed Nef-positive T lymphocytes predominantly in the follicles of mesenteric lymph nodes (MLNs). These data suggest that lymphatic tissues, including MLNs, contain major cellular reservoirs that cause rebound of plasma viremia upon cessation of therapy.

© 2011 Elsevier Inc. All rights reserved.

Introduction

Highly active antiretroviral therapy (HAART), which consists of three or more anti-HIV-1 drugs, is currently the primary choice of therapeutic intervention for HIV-1-infected individuals (Department of Health and Human Services (DHHS), 2011). The circulating viral loads in these patients are, in most cases, effectively suppressed below the limit of detection (<50 copies/ml of plasma) by HAART (Richman, 2001). However, the virus loads promptly rebound to pretreatment levels upon cessation of HAART (Chun et al., 1999), which suggests the persistence of viral reservoirs during the combined antiviral therapy. Therefore, to achieve a complete cure of HIV-1 infection, it is essential to eradicate these viral reservoirs.

Resting $CD4^+$ T lymphocytes have been identified as a viral reservoir (Chun et al., 1997; Finzi et al., 1997; Wong et al., 1997). These cells harbor intact viral genomes integrated into their chromosomes and produce infectious virus particles when they are reactivated in response to stimulation. It is noteworthy that the estimated half-life of a resting $CD4^+$ T cell is more than 44 months (Siliciano et al., 2003), which provides a theoretical basis for the source of the virus that rebounds upon cessation of long-term, successful HAART. Resting $CD4^+$ T lymphocyte is probably not the only reservoir of HIV-1. In the majority of patients on HAART, the rebounding viral genotypes detected in the plasma upon cessation of therapy were dissimilar to the genotypes extracted from resting $CD4^+$ T cells or from virus particles recovered from cells that were collected before interruption of the therapy (Chun et al., 2000).

Follicular dendritic cells (FDCs) have also been proposed as a viral reservoir (Spiegel et al., 1992). These cells are present in the follicles formed in all secondary lymphoid tissue. Rather than being infected with virus, FDCs retain infectious HIV-1 particles on the cell surface and transfer them to $CD4^+$ T lymphocytes (Burton et al., 2002). Since FDCs retain numerous virus particles, the genomes of which exhibit greater diversity than those in other tissues or cells and which reportedly hold infectious particles for months to years, it seems likely that these cells serve as archives of infectious virions (Keele et al., 2008).

The recently developed method for ultrasensitive detection of plasma viral burdens has revealed that patients who have HAART-controlled viremia (below the detection limit by clinical criteria; i.e., <50 copies/ml plasma) over several years still harbor minuscule

* Corresponding author at: Room 301, Molecular Biology Research Bldg, Institute for Virus Research, Kyoto University, 53 Kawahara-cho, Shogoin, Sakyo ward, Kyoto, Kyoto 606-8507, Japan. Fax: +81 75 761 9335.
E-mail address: tigarash@virus.kyoto-u.ac.jp (T. Igarashi).

0042-6822/$ – see front matter © 2011 Elsevier Inc. All rights reserved.
doi:10.1016/j.virol.2011.11.024

amounts of virion-associated RNA in the circulation (Palmer et al., 2008), suggesting ongoing viral replication, i.e., "residual viremia". The potential for ongoing HIV-1 replication during HAART is supported by evidence of *env* gene evolution in patients receiving HAART (Frost et al., 2001; Martinez et al., 1999), as well as the detection in patients on HAART of 1-LTR and 2-LTR circles, episomal HIV-1 cDNAs, the presence of which most likely reflects recent infection (Sharkey et al., 2000, 2005). A transient increase in the number of 2-LTR circles, probably reflecting an increase in the number of failed attempts to integrate into the host cell genome, was detected in approximately 30% of infected individuals who were receiving HAART, when an integrase inhibitor was added as treatment intensification (Buzon et al., 2010). Based on these lines of evidence, it is conceivable that certain cell types, as yet to be identified, allow productive replication of HIV-1 during HAART. Although HAART theoretically arrests *de novo* virus replication, these unidentified reservoirs appear to be refractory to the antiviral effects of the regimen through unknown mechanisms.

It is postulated that viral reservoirs in the host retain HIV-1 during HAART as follows: resting $CD4^+$ T lymphocytes store inducible viral genomes, FDCs archive infectious particles, and unidentified cells support productive viral replication cycles. It remains to be revealed whether other cell types serve as viral reservoirs using other mechanisms, and which cell type is the most important for sequestering HIV-1.

Peripheral blood samples from volunteer patients have been used in studies to identity HIV-1 reservoirs (Brennan et al., 2009; Chun et al., 2000; Sharkey et al., 2011). However, HIV-1 predominantly replicates in $CD4^+$ T lymphocytes in the lymphoid tissues (Embretson et al., 1993; Pantaleo et al., 1993), particularly the intestine, which is home to 70–90% of all lymphocytes in the body and which is severely affected during the acute phase of infection (Brenchley et al., 2004; Guadalupe et al., 2003), determining prognosis. Therefore a systemic analysis, in addition to existing studies on peripheral blood, would elucidate the mechanisms underlying rebound of plasma viremia upon discontinuation of HAART. Since it is unethical to collect various tissues from patients for analysis, an alternative model system is required. In this regard, the SIV/macaque model, which has been useful in understanding HIV-1 infection, is suitable for investigations of viral reservoirs using a systemic analysis (Dinoso et al., 2009; North et al., 2009).

Using the SIV239/macaque system, we investigated HIV-1 reservoirs during combined antiviral therapy (cART). First, we conducted a systemic analysis of SIV-infected Rhesus macaques that received cART for an extended period. SIV239 has been extensively used as a tractable animal model for HIV-1 in studies of replication, pathogenesis, and vaccine development. In addition, this virus causes almost complete depletion of $CD4^+$ T lymphocytes in the intestine (Veazey et al., 1998), as HIV-1 does in patients who suffer from AIDS.

Results

Establishment of anti-SIV239 cART regimen with oral administration

Before the experimental infection of macaques with SIV, we established an antiretroviral regimen that is applicable to SIV239 infection in the Rhesus macaque model. Given that NNRTIs do not suppress replication of SIV (Balzarini et al., 1995), anti-HIV-1 drugs belonging to this class were excluded from consideration. Regarding NRTIs, several studies have confirmed that Tenofovir (TDF) and its pro-drug PMPA are effective against SIV. Some studies have used Zidovudine (AZT) and Lamivudine (3TC) to suppress SIV replication *in vitro* and *in vivo* (Balzarini et al., 1995; Benlhassan-Chahour et al., 2003). Based on the results of these studies, we included TDF (Viread) and AZT/3TC (Combivir) in our regimen. Regarding protease inhibitors (PIs), Saquinavir (SQV) has been shown to be effective against SIV *in vitro* (Giuffre et al., 2003; Witvrouw et al., 2004). When we initiated this study, the anti-SIV efficacies of other commercially available PIs had not yet been reported. To determine which PI to include in our cART, we examined three commercially available PIs – SQV, Lopinavir/Ritonavir (LPV/RTV; Kaletra), and Atazanavir (ATV; Reyataz) – in the MT-4/MTT assay. This assay, which was originally developed to measure cell proliferation, was used to evaluate inhibition of virus-induced killing of human T-lymphoid MT-4 cells in the presence of increasing amounts of the drugs (Pauwels et al., 1988). Along with SIV239, HIV-1 IIIB was employed in the assay as a control. All of the compounds tested suppressed the activity of SIV239. The EC_{50} values for SQV were 18.5 nM against SIV and 22.7 nM against HIV-1 (Table 1 and Supplemental Fig. 1). The EC_{50} ratio, i.e., the EC_{50} value against SIV divided by the EC_{50} value against HIV-1, was 0.8 (Table 1). The EC_{50}s against SIV239 and the EC50 ratios of the other two drugs were: 52.2 nM and 1.5, respectively, for LPV/RTV; and 80.0 nM and 4.7, respectively, for ATV. Pharmacokinetic information on these drugs is available, and the half-life in the circulation in humans is: 1–2 h for SQV; 5–6 h for LPV/RTV; and 7 h for ATV (Department of Health and Human Services (DHHS), 2011). Taking into account the EC_{50}, the half-life (which defines the required frequency of administration to maintain the drug level), and cost-effectiveness, we included LPV/RTV in our regimen.

Drug administration was instituted *per os*, to effectively model the metabolism and pharmacokinetics of the antiviral drugs in patients. The dosage and administration of these drugs are described in the Materials and methods section. To assess whether a given dosage resulted in a measurable concentration of the drug in the circulation even after a long interval, blood samples were collected from six monkeys at 14 h after intake and the antiviral effect in plasma was determined by titration. The drug concentrations in the animals' blood ranged from 7.2 to 29.5 μM (LPV/RTV equivalent); these levels are 5- to 20-fold higher than those recommended for adult patients (1.5 μM for LPV/RTV equivalent) (Department of Health and Human Services (DHHS), 2011). Plasma samples from two representative animals, which had already been measured in the biological assay, were also subjected to HPLC. The results of the HPLC analysis revealed drug concentrations comparable to those determined by the biological assay: 16.1 μM for one animal (20.0 μM by the MTT assay) and 25.7 μM for the other animal (24.8 μM by the MTT assay), thus justifying our use of the biological assay to measure levels of antiviral activity in the circulation of SIV-infected animals during therapy. Based on these results, we finalized the regimen.

Efficacy of the cART regimen for macaques infected with SIV239

The establishment of the anti-SIV regimen enabled us to conduct animal experiments. Seven Rhesus macaques were inoculated intravenously with 2000 $TCID_{50}$ of the SIV239 virus stock. All animals exhibited an initial peak of viremia at 2 weeks post-inoculation (pi) (median, 2.2×10^7 copies/ml; range, $7.9–60.0\times10^6$ copies/ml, Fig. 1). At 8 weeks pi, when the viral loads decreased from the initial peak and plateaued (median, 1.3×10^5 copies/ml; range, $1.1–4.9\times10^5$ copies/ml), the cART was

Table 1
Efficacies of commercially available anti-HIV-1 protease inhibitors against SIV239 and HIV-1 IIIB.

Compounds	EC_{50}[a] (nM)		EC_{50} ratio[b]
	SIV239	HIV-1 IIIB	
Saquinavir	18.5	22.7	0.8
Lopinavir/ritonavir	52.2	35.6	1.5
Atazanavir	80.0	16.9	4.7

[a] 50% effective concentration.
[b] EC_{50} value against SIV239 divided by the EC_{50} value against HIV-1 IIIB.

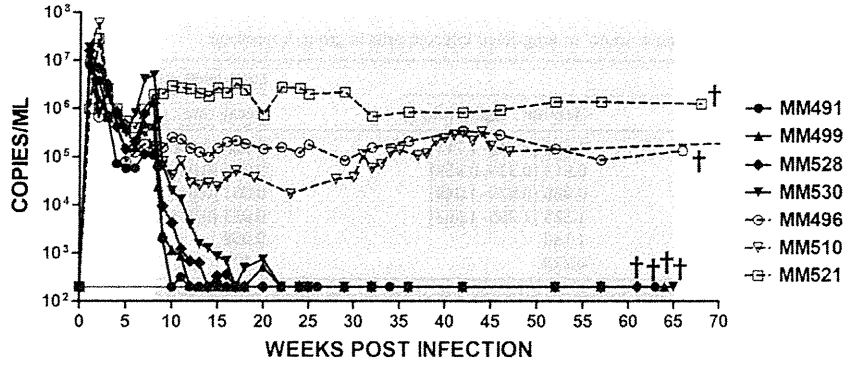

Fig. 1. Effects of cART on plasma viral loads. Seven Rhesus macaques were inoculated with SIV239. Four animals, MM491, MM499, MM528, and MM530 (solid lines), were treated with cART (shaded areas). Animals MM510, MM496, and MM521 (dotted line) served as untreated controls. The detection limit of our RT-PCR assay is 200 RNA copies/ml, and samples with levels below the level of detection are plotted as 200 RNA copies/ml. †, time of euthanasia.

administered to four of the monkeys (MM491, MM499, MM528, and MM530; designated as group A).

Upon drug administration, the plasma viral RNA (vRNA) levels in these animals promptly started to decrease. There was an inverse inclination between set point plasma vRNA load and duration to suppress vRNA to the detection limit (200 copies/ml). The vRNA of MM491, whose set point viral RNA level was the lowest in the group 1.1×10^5 copies/ml, fell below the detection limit in 2 weeks. MM499 and MM528, whose plasma vRNAs were 4.4×10^5 and 1.3×10^6 copies/ml at the initiation of cART, took 5 and 6 weeks, respectively. After nine weeks of treatment, the viral burden of MM530, which had the highest level in the group at 4.9×10^6 copies/ml, was undetectable. Plasma vRNA levels of all animals on cART had fallen below the limit of detection by 17 weeks pi. When HAART was applied to SIV/pigtailed macaque or RT-SHIV/rhesus macaque models, it took 8 and 18 weeks, respectively, to suppress circulating vRNA to below the detection limit (Dinoso et al., 2009; North et al., 2009). When considering variables from previous studies, including virus strain, drug combinations, detection limit of vRNA measurement, and initiation of treatment of these studies, it is conceivable that the cART approach devised in the current study is as potent in terms of the progress to viral containment.

To relate our results to previous studies on vRNA declines for HIV-1 and SIV following antiviral therapy, we examined the levels of viremia in our infected monkeys during the first few weeks after the initiation of therapy (Table 2 and Supplemental Fig. 2). Each individual monkey followed a similar pattern of viral decay: an initial rapid and exponential reduction by almost 2.5 orders of magnitude (comprising the first phase, which is presumably associated with short-lived infected cells), followed by a slower exponential decline of 1.5 orders of magnitude (the second phase, which is presumably associated with long-lived infected cells). The observed biphasic decay of viral burdens was consistent with previous findings from studies on SIV models and patients with HIV-1 (Dinoso et al., 2009; Murray et al., 2007; Perelson et al., 1997; Perelson and Nelson, 1999). Decay rates for the first and second phases were deduced by employing mathematical modeling (Table 2). The decay rates of the first phase ranged from 0.495 (for MM491) to 0.853 (for MM499), and those of the second phase ranged from 0.028 (for MM491) to 0.089 (for MM499). The decay rates of plasma vRNA loads during the first phase in patients with HIV-1 on HAART, consisting of LPV/RTV, Efavirenz, 3TC, and TDF, exhibited comparable numbers to those in the current study, ranging from 0.6 to 1.4 (Markowitz et al., 2003). Mean half-lives of ($\log 2/a=$) 1.13 for the first phase and ($\log 2/\mu_M$) 14.24 days for the second phase were comparable to those observed in patients with HIV-1 on HAART. Half-lives of HIV-1 RNA in the circulation of HIV-1-infected patients on suppressive ART, consisting of Indinavir and Efavirenz, ranged from 0.6 to 2.0 days for the first phase and 5.2 to 35.6 days for the second phase (Havlir et al., 2003). Comparison of the viral decay rates derived in the current study with those derived in previous reports (Perelson et al., 1997) gave statistically insignificant results ($P=0.667$ for the first phase, and $P=0.662$ for the second phase). These results suggest that the virologic response of SIV infected Rhesus macaques to cART, as reported in a recent study (Dinoso et al., 2009), is comparable to the response of HIV-1-infected patients to HAART.

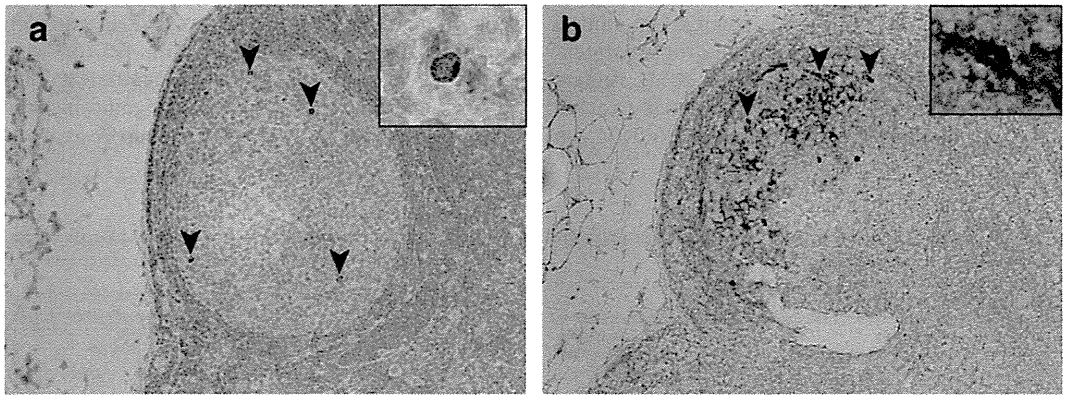

Fig. 2. Nef-expressing cells detected in the iMLNs of animal MM511. (a) The section was stained with the anti-SIV Nef mouse monoclonal antibody. (b) Juxtaposition of Nef-expressing cells and CD35-positive FDCs in the follicle of an iMLN from MM511. The sample was stained using the anti-SIV Nef mouse monoclonal antibody (brown) and the anti-CD35 mouse monoclonal antibody (blue). Original magnification, ×40. The insets contain a higher-magnification, ×126 equivalent (original magnification, ×63).

Table 2
Decay rate and half-life derived by mathematical modeling of short- or long-lived infected cells in group A monkeys.

Animal ID	Short-lived infected cells		Long-lived infected cells	
	Decay rate : a (day^{-1})	Half-life : $log2/a$ (days)	Decay rate : μ_M (day^{-1})	Half-life : $log2/\mu_M$ (days)
MM491	0.495 [0.405–0.605][a]	1.400 [1.146–1.711]	0.028 [0.000–0.141]	24.76 [4.916–∞]
MM499	0.853 [0.807–1.287]	0.813 [0.539–0.859]	0.089 [0.083–0.100]	7.753 [6.931–8.402]
MM528	0.707 [0.661–0.746]	0.980 [0.929–1.049]	0.061 [0.045–0.070]	11.44 [9.846–15.44]
MM530	0.523 [0.372–0.575]	1.325 [1.205–1.863]	0.053 [0.035–0.064]	13.00 [10.85–19.86]
Mean	0.645	1.130	0.058	14.24
S.D.	0.168	0.279	0.025	7.351

[a] Values in parentheses represent the lower and upper 68% confidence intervals, calculated by a bootstrap method in which each experiment was simulated 1000 times.

Patients with HIV-1 on HAART exhibit undetectable levels of plasma vRNA (typically less than 50 copies/ml) when the therapy works as expected. To estimate suppression levels achieved by the regimen used in the current study, selected plasma samples with adequate volume from animals in group A were subjected to another quantitative real-time PCR assay with a lower detection limit. Using 1.5-ml plasma samples, which were collected at 29, 42, and 52 weeks pi, and at euthanasia, particle-associated vRNA was extracted and amplified. All of these samples yielded less than 20 copies/ml of vRNA loads (Table 3), except for those collected at 42 and 52 weeks pi (44 and 47 copies/ml, respectively) from MM530, which exhibited the highest plasma vRNA at the start of cART (4.9×10^6 copies/ml) and required the longest duration to suppress vRNA to 200 copies/ml (9 weeks). These results confirm that the regimen established in the current study is as suppressive as those applied to patients. Based on the progression to viral containment, decay rates, and suppression levels, we concluded that the cART established in the current study is comparable to therapies used to treat patients with HIV-1 and suitable to pursue viral reservoirs during therapy. The suppressed viral burdens of the treated animals were maintained below the limit of detection throughout the course of treatment (up to 52 weeks). In contrast, the viral burdens of the untreated animals (MM496, MM510, and MM521) remained at $>1.0\times10^5$ copies/ml until the day of necropsy (Fig. 1). Assuming a limit of viral detection of 200 copies/ml, there was a statistically significant difference in the plasma vRNA levels between the two groups of animals at week 42 ($P<0.05$).

During the entire course of cART, the levels of antiviral activity in the plasma samples of animals MM491, MM528, and MM530 assessed by MT-4/MTT assay were above the recommended trough level for adult patients (for MM491: range, 3.5–17.8 μM LPV/RTV equivalent; for MM528: range, 6.0–24.9 μM LPV/RTV equivalent; for MM530: range, 8.2–14.2 μM LPV/RTV equivalent) (Table 4). Even in the remaining animal, MM499, in which the circulating concentration of the activity was below the recommended trough level at the two time-points tested, at 10 weeks pi and at autopsy, during the course of antiviral therapy, the plasma vRNA levels were below the limit of detection. None of the treated animals exhibited a transient surge in vRNA level during the entire course of the therapy. Certain clinical conditions are known to be side-effects of antiviral drug treatment (Department of Health and Human Services (DHHS), 2011). Among the drugs employed in the present study, TDF potentially causes renal complications (Van Rompay et al., 2004) and LPV/RTV can induce abnormal lipid metabolism. In general, no significant adverse effects were noted for the drugs employed in the present study. We conclude that the antiretroviral therapy regimen established in the current study is as effective as the combined antiretroviral therapy applied to patients with HIV.

Higher titers of vRNA were detected in the lymphoid tissues of virus-infected animals undergoing antiretroviral therapy

The establishment of an effective antiretroviral therapy regimen for SIV-infected monkeys was a prerequisite for the identification of virus reservoirs during combined antiviral therapy. To this end, we considered two important questions: 'Is virus replication maintained during the therapy?', and 'If active virus replication persists, are there particular anatomic compartments that allow preferential virus replication?'

To answer these questions, we looked for the presence of vRNA in a variety of tissues collected from animals receiving cART over a period of 1 year. Total RNA was extracted from each tissue and subjected to real-time reverse transcription (RT)-PCR. Table 5 summarizes the results of RT-PCR for four animals in group A that were subjected to analysis at the end of the 1-year cART regimen, along with a representative animal that was not given treatment (MM521); all the animals were euthanized at between 61 and 68 weeks pi. In the untreated monkey (MM521), vRNA was detected in all the tissues examined, with the exception of the brainstem. In the lymphoid tissues, higher titers of vRNA (approximately 1.0×10^8 copies/μg total RNA) were detected. In the gastrointestinal tract, lungs, and vagina, in which the resident $CD4^+$ T-lymphocyte population consists mainly of $CCR5^+$ memory cells (the preferred target of HIV-1 and SIV) (Douek et al., 2003; Meng et al., 2000; Veazey et al., 2000), the vRNA titers were approximately 1.0×10^6 copies/μg of total RNA. Lower levels of vRNA were detected in the non-lymphoid tissues (heart, liver, and kidneys) and the central nervous system (cerebrum and cerebellum).

In the group A macaques, the vRNA titers in several tissues were much lower than those found in the untreated animals. The non-lymphoid tissues and central nervous system did not contain measurable amounts of vRNA. Low levels of vRNA were detected in the effector sites, such as the intestine (up to 6.5×10^4 copies/μg total RNA), lungs, and vagina (up to 6.5×10^3 copies/μg total RNA). Statistical analysis of vRNA burdens revealed significant reductions in the jejunum and rectum of animals in group A as compared to those of

Table 3
Plasma viral loads of selected samples measured by RT-PCR with a lower detection limit (20 copies/ml) in group A animals during cART.

Animals ID	Plasma viral loads (copies/ml)			
	29 wpi	42 wpi	52 wpi	At autopsy[a]
MM491	<20	<20	<20	<20
MM499	<20	<20	<20	<20
MM528	<20	<20	<20	<20
MM530	<20	44	47	<20

[a] MM491, 63 wpi; MM499, 64 wpi; MM528, 61 wpi; MM530, 65 wpi.

Table 4
Antiretroviral activities detected in the blood of animals in group A during cART.

Animals ID	Drug concentration (μM)[a]					
	10 wpi	20 wpi	32 wpi	42 wpi	56 wpi	At autopsy[b]
MM491	3.5	15.9	12.1	17.8	7.9	5.2
MM499	0.6	2.3	4.4	11.4	1.7	0.9
MM528	16.0	24.9	6.6	7.7	6.0	9.3
MM530	9.4	12.4	8.2	14.2	11.3	11.3

[a] LPV/RTV equivalent concentration.
[b] MM491, 63 wpi; MM499, 64 wpi; MM528, 61 wpi; MM530, 65 wpi.

Table 5
Viral RNA burdens in various tissues collected from SIV-infected macaques.

Tissues	vRNA levels (copies/μg total RNA)				
	Treated with cart				Untreated
	MM491 <200 copies/ml[a]	MM499 <200 copies/ml[a]	MM528 <200 copies/ml[a]	MM530 <200 copies/ml[a]	MM521 1.2×10^6 copies/ml[a]
Non-lymphoid tissues					
Heart	< 2900	< 2900	< 2900	< 2900	3.0×10^3
Liver	< 2900	< 2900	< 2900	< 2900	8.8×10^4
Kidney	< 2900	< 2900	< 2900	<2900	2.1×10^6
CNS tissues					
Cerebrum	< 2900	< 2900	< 2900	< 2900	1.1×10^6
Cerebellum	< 2900	< 2900	< 2900	< 2900	4.5×10^3
Brain stem	< 2900	< 2900	< 2900	< 2900	< 2900
Effector sites					
Lung	4.7×10^3	4.1×10^3	<2900	< 2900	1.0×10^5
Vagina	6.5×10^3	< 2900	<2900	2.9×10^3	1.3×10^5
Jejunum	5.0×10^3	3.1×10^3	1.1×10^4	7.4×10^3	1.7×10^6
Ileum	5.2×10^3	4.0×10^3	7.7×10^3	< 2900	1.4×10^6
Colon	1.8×10^4	< 2900	6.5×10^4	8.3×10^3	2.0×10^8
Rectum	2.9×10^3	< 2900	6.0×10^3	9.9×10^3	4.7×10^6
Lymphoid tissues					
Spleen	2.6×10^4	5.0×10^3	5.4×10^3	6.2×10^3	3.4×10^8
Thymus	< 2900	< 2900	N.D.	2.0×10^5	2.9×10^4
Iliac LN	5.8×10^4	6.9×10^3	1.5×10^4	3.6×10^4	1.6×10^8
Inguinal LN	< 2900	2.4×10^4	2.4×10^4	2.3×10^5	6.9×10^7
Axillary LN	8.6×10^4	7.2×10^3	3.1×10^4	2.1×10^5	7.6×10^7
iMLN	1.0×10^5	8.8×10^4	< 2900	2.9×10^5	1.0×10^8
sMLN	1.3×10^5	5.7×10^4	3.4×10^4	2.4×10^5	2.3×10^8
Submandibular LN	6.2×10^4	2.9×10^4	1.6×10^4	5.6×10^3	3.9×10^7
Bronchial LN	1.5×10^5	5.3×10^4	3.1×10^4	3.8×10^5	1.1×10^8
Splenic LN	2.5×10^5	4.3×10^4	7.3×10^3	2.0×10^5	9.8×10^7

N.D., no data; CNS, central nervous system; LNs, lymph nodes; iMLNs, inferior mesenteric lymph nodes; sMLNs, superior mesenteric lymph nodes.
Viral RNA (vRNA) levels greater than detection limit (2900 copies/μg total RNA) are represented in bold. vRNA levels are coded in grayscale as follows: white boxes, <2900; light-gray boxes, $<1.0\times10^5$; dark-gray boxes, $<1.0\times10^7$; black boxes, $>1.0\times10^7$.
[a]Viral loads in plasma.

untreated controls ($P=0.03$), indicating that cART suppressed vRNA expression in those tissues, although incompletely. Compared to the above-mentioned tissues, higher levels of vRNA (approximately 1.0×10^5 copies/μg of total RNA) were detected in the lymphoid tissues. Of note, both the superior and inferior mesenteric lymph nodes (sMLNs and iMLNs, respectively) were among the tissues that contained the highest titers of vRNA in animals on cART. Statistical analysis of vRNA in the lymphatic tissues also revealed significant suppression in group A as compared to controls (iliac and submandibular lymph nodes and iMLNs, $P=0.03$).

To identify the cell type(s) that support vRNA synthesis and, potentially, allow viral proteins to be produced during ART, we prepared tissue sections from the animals in group A and subjected them to *in situ* hybridization (ISH) and immunohistochemistry (IHC). While these tissues yielded no positive signals, the same staining techniques detected vRNA-positive cells and viral-protein-positive cells in tissue sections prepared from untreated animals (data not shown).

In summary, our initial questions were resolved as follows: the presence of vRNA in the gut, lungs, vagina, and lymphoid tissues indicated active viral replication in animals that were treated with cART for 1 year, and the lymphatic tissues allowed preferential viral replication in these animals.

SIV Nef-producing T lymphocytes predominated in the follicles of the MLNs from an animal that exhibited rebound of plasma viremia upon cessation of cART

Quantitative PCR analysis of vRNA in a variety of tissues collected from SIV-infected animals that were on prolonged chemotherapy (i.e., the animals in group A) indicated that the lymphatic tissues acted as the anatomic compartment for active virus replication during antiretroviral therapy. However, we were unable to identify histochemically any vRNA-positive or viral-protein-positive cells in the tissue sections prepared from these animals. This discrepancy was likely due to the lower sensitivity of these staining techniques as compared to PCR. We assumed that cessation of ART would result in rebound of plasma viremia, thereby promoting the transcription and translation of viral genes to levels detectable by the histochemical staining techniques employed in the present study. Based on this assumption, we took advantage of the rebound of plasma viremia as a surrogate approach to identify the viral reservoir(s) during cART. Thus, two Rhesus macaques (MM508 and MM511, designated as group B animals) were inoculated with the same SIV239 virus stock as was used to inoculate the group A animals. The group B animals exhibited an initial peak of viremia at 2 weeks pi (range, 7.7–8.4×10^7 copies/ml; Table 6), and the viral loads decreased and stabilized from 8 wpi onwards. Upon initiation of cART at 38 wpi, the levels of virus decreased rapidly and eventually fell below the limit of detection. The suppressed viral burdens were maintained until cessation of the treatment at 46 weeks pi. We attempted to determine the time-point at which the levels of viral gene transcription and translation were just above the detection limit of our staining. Since we envisioned that rebound of plasma viremia would take place within 2 weeks of interruption of therapy, animals were euthanized for necropsy on Day 10 after cessation of cART. The viral load in the plasma of animal MM511 was 1400 copies/ml, while that of animal

Table 6
Viral loads in plasma samples of animals in group B.

Animal ID	Plasma viral loads (copies/ml)					
	0 wpi	2 wpi	8 wpi	38 wpi	46 wpi	At autopsy[a]
MM508	<200	8.4×10^6	2.6×10^5	3.8×10^4	<200	<200
MM511	<200	7.7×10^6	3.1×10^5	1.1×10^5	<200	1.4×10^3

The animals were treated with cART from 38 wpi to 46 wpi.
[a] 47.5 wpi.

Table 7
Viral RNA burdens in various tissues collected from animals in group B.

Tissues	vRNA levels (copies/μg total RNA)	
	MM508 PVL, <200 copies/ml	MM511 PVL, 1400 copies/ml
Non-lymphoid tissues		
Heart	< 2900	< 2900
Liver	< 2900	< 2900
Kidney	< 2900	< 2900
CNS tissues		
Cerebrum	< 2900	< 2900
Cerebellum	< 2900	< 2900
Brain stem	< 2900	< 2900
Effector sites		
Lung	< 2900	< 2900
Vagina	< 2900	N.D.
Upper intestinal tract	< 2900	< 2900
Lower intestinal tract	< 2900	< 2900
Lymphoid tissues		
Spleen	**2.0×10^5**	**7.4×10^5**
Thymus	<2900	<2900
Iliac LN	**1.4×10^4**	**3.5×10^5**
Inguinal LN	<2900	**5.3×10^5**
Axillary LN	**1.9×10^4**	**1.3×10^6**
iMLN	**1.3×10^5**	**1.6×10^6**
sMLN	**8.4×10^3**	**1.5×10^6**
submandibular LN	**1.1×10^5**	**9.4×10^5**
Bronchial LN	**1.1×10^4**	**9.5×10^5**
Splenic LN	**9.9×10^4**	N.D.

PVL, plasma virus load; N.D., no data; CNS, central nervous system; LNs, lymph nodes; iMLNs, inferior mesenteric lymph nodes; sMLNs, superior mesenteric lymph nodes. Viral RNA (vRNA) levels greater than detection limit (2900 copies/μg total RNA) are represented in bold. vRNA levels are colored in grayscale as follows: white boxes, <2900; light-gray boxes, $<1.0 \times 10^5$; dark-gray boxes, $<1.0 \times 10^7$.

MM508 was below the limit of detection (Table 6). Thus, one animal was exhibiting rebound of plasma viremia while the other animal had not yet reached that stage when they were killed for analysis.

The overall tendency of the vRNA distribution in the group B animals was similar to that observed in the group A animals, with the titers being somewhat higher in group B. Higher levels of vRNA ($>1.0 \times 10^4$ copies/μg total RNA) were detected exclusively in the lymphoid tissues (Table 7). In MM511, the highest level of vRNA was detected in the MLNs ($>1.0 \times 10^6$ copies/μg total RNA). MM508, in which the plasma viral load was below the limit of detection at euthanasia, contained high levels of vRNA ($>1.0 \times 10^5$ copies/μg of total RNA), but only in the spleen and iMLN.

Based on the increased levels of vRNA transcription, we hypothesized that higher levels of viral proteins were synthesized in these two animals (MM508 and MM511) than in the group A animals. We subjected all the lymphoid tissues collected from these two animals to IHC, to identify viral-protein-producing cells. First, we focused on MM511, which exhibited higher viral titers in the plasma and lymphoid tissues than MM508, and stained tissue sections from this animal with anti-Nef antibodies. IHC yielded Nef-positive cells (Fig. 2). The viral-protein-positive cells were mainly localized to the globular architecture in the lymph node cortex, most likely the lymphoid follicles, and the Nef-positive cells bore morphologic characteristics similar to those of T lymphocytes (Fig. 2a). To clarify the architecture within which the Nef-producing cells were detected, we conducted combined IHC with an anti-Nef antibody (visualized with DAB) and an antibody directed against CD35 (visualized with VECTOR Blue). CD35 is a cell surface marker for FDCs, which are found exclusively in the follicles of the secondary lymphoid tissues. The combined staining showed that Nef-positive cells and FDCs were present in the same globular architecture, suggesting that the viral-protein-producing cells were predominantly located in the follicles of the lymph nodes of this animal. Moreover, staining revealed that the Nef-producing cells were juxtaposed on the FDCs (Fig. 2b).

To confirm the identity of the viral-protein-expressing cells, we conducted combined immunofluorescence staining with an anti-Nef antibody (visualized with Alexa Fluor 488) and an anti-CD3 antibody (visualized with Alexa Fluor 594). After extensive observations of the stained sections under the microscope, we detected Nef-positive cells in 16/305 sections prepared from a variety of lymphatic tissues collected from animal MM511, and these viral-protein-expressing cells were all positive for CD3 (Fig. 3 and Table 8). Of these 16 sections, 12 were prepared from MLNs and 4 from other anatomical

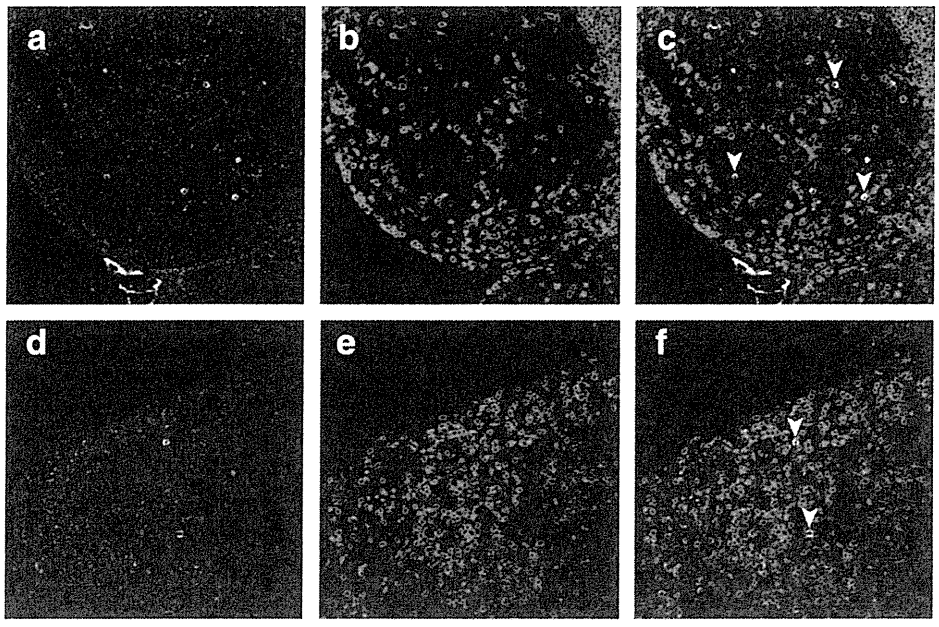

Fig. 3. Nef-positive T lymphocytes in the MLN of animal MM511. Tissue sections were stained using the anti-SIV Nef mouse monoclonal antibody (green, a and d) and the anti-CD3 rabbit polyclonal antibody (red, b and e). (c) Superimposed image of a and b. Nef-positive T cells are clustered in the follicles of the iMLN. (f) Superimposed image of d and e. The T cell is detected in the paracortical area of the sMLN. Original magnification, ×40.

compartments. The viral-protein-producing cells in the follicles constituted around 75% of all the positive cells detected. In some sections, Nef-positive cells were clustered in the follicles (Fig. 3c).

In animal MM508, which was subjected to analysis before rebound of plasma viremia had taken place, the staining revealed a single Nef-positive cell that was also positive for CD3 (data not shown). The frequency of positive cells in this animal was substantially lower (one positive cell in 136 sections) than that in MM511.

In summary, in the animal that exhibited rebound of plasma viremia after cessation of cART, almost all the viral-protein-synthesizing cells, presumably productively infected cells, that were detected in the MLNs were identified as T lymphocytes, most likely $CD4^+$ T cells. The vast majority of the virus-infected T cells were observed in the lymphoid follicles during rebound of plasma viremia (Table 8).

Discussion

The presence in infected individuals of HIV-1 viral reservoirs that persist during HAART impedes curing and complete eradication of the virus. While studies have been conducted into the identity and properties of the HIV-1 reservoirs (Brennan et al., 2009; Chun et al., 2000; Sharkey et al., 2011), much remains to be learnt. We reasoned that systemic analyses of infected individuals who were undergoing intensive ART would advance the characterization of the viral reservoirs (Dinoso et al., 2009; North et al., 2009). Therefore, we analyzed SIV-infected Rhesus macaques that underwent cART for 1 year. The major finding of the current study is that lymphatic tissues, including MLNs, contained higher numbers of cellular virus reservoirs that potentially cause rebound of plasma viremia upon cessation of cART. This assertion is based on the following observations: the lymphatic tissues contained the highest levels of vRNA in all the animals, regardless of cART, and the viral-protein-expressing T cells were localized predominantly to the MLNs of the animal that exhibited rebound of plasma viremia after cessation of cART.

We finalized the drug dosages to be administered by monitoring plasma trough levels of antiviral activity at 14 h post-consumption. During this process we discovered that the drug metabolism of monkeys is somewhat higher than that of humans. To fine-tune the drug concentrations in the circulation, 50% of the dosage established in the present study, corresponding to 150% of the dosage for a 60-kg adult patient, was given to the same animals. The circulating drug concentration at 14 h post-consumption yielded no measurable net antiviral activity (data not shown). Therefore, it is necessary to determine an appropriate dosage for each drug prior to administration to animals. In this regard, one of the monkeys in group A, MM499, exhibited fluctuating antiviral activity during the therapy. At 10 and 64 weeks pi, the antiviral activity in the blood was below the recommended trough level for patients (1.5 μM) (Table 4). Despite the fluctuation of antiviral activity, the viral burden of this animal was maintained below the limit of detection during the therapy, and systemic analysis revealed levels of vRNA that were comparable to those detected in the other three animals in group A (Table 5). That the other three animals also exhibited fluctuating concentrations of the drug in the circulation underlines the importance of monitoring antiviral activity in circulation during therapy, to ensure that the administration schedule produces the expected antiviral activity.

RT-PCR analyses revealed that lymphatic tissues contained higher titers of vRNA than the other tissues in 4/4 SIV-infected macaques in group A, and 2/2 animals in group B followed the same distribution of vRNA (Tables 5 and 7). In SIV-infected monkeys treated with cART, the Lamivudine concentration was more than 300-fold higher in the gastrointestinal tract than in the peripheral lymph nodes (Bourry et al., 2010). The finding of Bourry et al. explains our observation that chemotherapy was more effective at suppressing virus replication in the intestine than in the lymph nodes. It is possible that lymphatic tissues serve as viral sanctuaries, especially when the amount of drug accumulated in the tissues is insufficient to suppress virus replication. It should be noted that while viral load and drug concentration in the plasma are easily monitored, they do not reflect precisely the virus replication/drug distribution in specific important anatomic compartments.

Our results are also in good agreement with the results reported by North et al., who performed a thorough analysis of a variety of tissues collected from RT-SHIV-infected animals that were receiving combined anti-viral therapy (North et al., 2009). The authors employed RT-SHIV, which is a chimeric virus that carries the HIV-1-derived RT gene on the backbone of SIV239, to model HAART to patients, in the context of SIV, since non-nucleotide reverse-transcriptase inhibitors (NNRTIs), one of the core components of HAART, do not suppress reverse transcription mediated by SIV RT (Balzarini et al., 1995). Although the cART regimen devised in the current study is unlike the HAART administered to patients, especially with respect to the employment of certain drugs, the viral decay rate in the circulation (calculated based on a two-compartment model) is comparable to that observed in patients treated with the multi-drug regimen (Murray et al., 2007; Palmer et al., 2008; Perelson et al., 1997) (Table 2 and Supplemental Fig. 2). Therefore, it is implied that the lymphatic tissues may harbor higher titers of vRNA in HIV-1-infected patients on HAART, despite the viral burdens in the circulation are clinically non-detectable. The caveat is that the animals in the current study were on treatment for up to 1 year only, which is a considerably shorter treatment period than that of patients who have achieved successful virus containment since the beginning of the HAART era. Given that the desired concentration of the drug may not be reached in the lymphatic tissues, it is necessary to devise a way to deliver in a preferential manner either antiviral drugs or a specific injury to these compartments, in combination of HAART, to achieve eradication of the virus, which is a crucial step toward a complete cure for HIV-1 infection.

Histochemical analyses revealed that the SIV Nef protein was expressed in T lymphocytes predominantly resident in the follicles formed in the MLNs of animal MM511, which exhibited viral rebound after cessation of cART (Fig. 3 and Table 8). Active virus replication in the follicles of lymph nodes has been described (Folkvord et al., 2005). Previous studies have suggested that lymphatic follicles serve as preferred sites of virus replication, probably *via* FDCs and sequestration of virus-infected cells from cytotoxic T lymphocytes (CTLs). FDCs, which may interact with $CD4^+$ cells within the "enclave", retain infectious virus particles and produce TNF-α, which promotes HIV replication (Thacker et al., 2009). HIV-1-specific CTLs fail to accumulate within lymphoid follicles, allowing unchecked virus replication in this architecture (Connick et al., 2007). Taken together, these findings support our observations of active viral protein synthesis in the lymphoid follicles.

The present study does not identify definitively the viral reservoirs. However, it does not rule out any of the proposed candidate reservoirs: resting $CD4^+$ T lymphocytes, FDCs, and unidentified cells involved in ongoing virus replication during therapy. To place our results in the context of current thinking regarding putative viral reservoirs, we make the following important points:

Table 8
Numbers of immunohistochemistry sections examined from macaques in group B.

Nef expressing T cells	Number of sections subjected				
	MM508		MM511		
	MLN	Non-MLN	MLN	Non-MLN	Total
Present in the follicles	0	0	9	3	12
Present in the paracortical area	1	0	3	1	5
Absent	50	85	34	255	424

MLNs; mesenteric lymph nodes.

North et al.(2009) detected proviral DNA in the resting $CD4^+$ T-lymphocyte fraction prepared from MLNs. Dinoso et al.(2009) recovered replication-competent viruses in the cell fraction. It is possible that the Nef-positive cells detected in the current study were reactivated upon stimulation, thereby prompting resumption of the virus replication cycle; the progeny viral particles from these cells would initiate multiple rounds of replication in the T cells of the paracortical area and the follicles of the lymph nodes.

We detected FDCs juxtaposed on the Nef protein-positive T lymphocytes. This observation is not definitive evidence that FDCs transmit infectious viral particles to $CD4^+$ T cells. Based on our observations, we hypothesize that FDCs transmit virus to $CD4^+$ T cells or stimulate infected cells, so as to initiate viral rebound. An important caveat is that the animal in question was treated for only 8 weeks. Since FDCs are known to retain virus particles with their infectivity intact for a certain period of time (Keele et al., 2008), it would be informative to determine whether the interaction between these two cell types occurs in animals that exhibit rebound after a prolonged period of therapy, followed by cessation.

Although we have no direct evidence that unknown cells are involved in ongoing viral replication during therapy, higher titers of vRNA were detected in the lymphatic tissues, primarily the MLNs, which suggests that certain cell types in this compartment allow viral replication during chemotherapy. It is likely that the levels of transcription of viral genes and of subsequent translation are too low to be detected by the staining techniques employed in the current study.

Based on our results, we postulate the following sequence of events after the cessation of HAART in individuals infected with HIV-1: in the follicles of the lymph nodes, such as MLNs, viruses that are preserved in certain forms, such as intact genomes and infectious particles, and with low-level ongoing replication, resume a productive replication cycle, preceding other anatomical compartments, when the concentration of the antiviral drug declines due to discontinuation of therapy; thereafter, other anatomic compartments resume productive viral replication owing to weakened containment of the virus and higher accumulations of the drugs. The progeny viral particles produced from the tissues subsequently enter the circulation and cause rebound of plasma viremia, i.e., systemic viral replication.

Considering that the state-of-the-art histochemical staining still has lower sensitivity than PCR and that the vRNA distributions for animals on ART and those with rebound of plasma viremia are similar, analyses of animals undergoing rebound of plasma viremia after discontinuation of therapy could serve as a surrogate approach to study virus reservoirs during HAART.

Fortunately, we captured ongoing rebound of plasma viremia in animal MM511, whose viral burden was above the detection limit defined by the current staining technique. Further fine-tuning in the duration of therapy and timing of analysis after cessation would provide better clues to the identity of virus reservoirs.

Materials and methods

Cells

Human embryonic kidney-derived 293T cells were cultured in Dulbecco's modified Eagle's medium (D-MEM; Invitrogen, Carlsbad, CA) that was supplemented with 10% fetal bovine serum (FBS; HyClone Laboratories, Logan, UT) and 2 mM L-glutamine. Human T-lymphoid MT-4 (Harada et al., 1985), Molt-4 (Koyanagi et al., 1986), and M8166 (Shibata et al., 1991) cells were cultured in RPMI 1640 medium (Invitrogen) that was supplemented with 10% FBS, 2 mM sodium pyruvate, and 4 mM L-glutamine (R-10). Rhesus macaque PBMCs were prepared from whole blood that was anticoagulated with EDTA in lymphocyte separation medium (Nakalai Tesque, Kyoto, Japan). PBMCs were resuspended in R-10 medium that was supplemented with 40 μg/ml gentamicin, 50 μM 2-mercaptoethanol, and 25 μg/ml concanavalin A (Sigma-Aldrich, St. Louis, MO), and cultured for 16–20 h at 37 °C. Before virus infection, the cells were cultured for an additional 2 days in R-10 medium that was supplemented with 40 μg/ml gentamicin, 50 μM 2-mercaptoethanol, and 100 IU/ml recombinant human IL-2 (Imunace; Shionogi, Osaka, Japan).

Viruses

The stock of SIV239 used in the tissue culture and animal experiments was prepared in Rhesus macaque PBMCs inoculated with the supernatant of a 293T-cell culture that was transiently transfected with full-length infectious molecular clones of the virus (Kestler et al., 1990). A stock of HIV-1 IIIB (Popovic et al., 1984) was prepared from the supernatant of a Molt-4 cell culture that was chronically infected with the virus. The SIV239 stock was titrated by infection of M8166 cells, and the number of infectious units was calculated by a method described previously (Reed and Muench, 1938).

Animal experiments

Female Rhesus macaques of Chinese or Indian origin, 4 kg in body weight, were used for experimental infection with SIV239. Phlebotomy and virus inoculation were carried out under anesthesia by intramuscular injection of a mixture of ketamine chloride (Ketalar; Daiichi Sankyo, Tokyo, Japan) at 5–10 mg/kg and xylazine chloride (Celactal; Bayer Healthcare, Leverkusen, Germany) at 1.5–2.0 mg/kg. For virus infection, animals were inoculated intravenously with 2000-times the 50% tissue culture infectious doses ($TCID_{50}$) of SIV239. Animal experiments were conducted in a biosafety level 3 animal facility, in compliance with institutional regulations approved by the Committee for Experimental Use of Nonhuman Primates of the Institute for Virus Research, Kyoto University, Kyoto, Japan.

Extraction of active components from drug tablets or plasma

Saquinavir (Invirase; Chugai Pharmaceutical, Tokyo, Japan), Lopinavir/Ritonavir (Kaletra; Abbott Laboratories, Abbott Park, IL), and Atazanavir (Reyataz; Bristol-Myers Squibb, New York, NY) were purchased from their respective sources. Drug tablets were pulverized with a pestle and mortar and dissolved in dimethyl sulfoxide (DMSO; Wako Pure Chemical Industries, Osaka, Japan). The concentration of each drug in DMSO was adjusted to 100 μg/ml with RPMI 1640 medium. To simulate the conditions of the drugs in the blood, the drug solutions were diluted 10-fold with normal plasma from Rhesus macaque. The drug extract was subsequently deproteinized by mixing with methanol/acetonitrile (1:1). The soluble fraction was evaporated, subsequently reconstituted in RPMI 1640 medium, and adjusted to a concentration of 20 μg/ml. Plasma samples collected from the animals were deproteinized, evaporated, and reconstituted as described above. The efficacy of the extraction employed in the current study ranged from 30 to 50% when assessed using the anti-HIV-1 drugs AZT, SQV, and RTV (data not shown).

Virus inhibition assay (MT-4/MTT assay)

The efficacies of the PIs against SIV were assessed as described previously (Sato et al., 1995), with minor modifications. Briefly, aliquots of 5×10^3 MT-4 cells were dispensed into 96-well round-bottomed tissue culture plates. Serially diluted extracts of the HIV-1 PIs or extracts of animal plasma samples were incubated with the cells in quadruplicate at 37 °C for 1 h. The cells were then inoculated with 1.8×10^3 $TCID_{50}$ of SIV239 or 0.9×10^2 $TCID_{50}$ of HIV-1 IIIB (multiplicity of infection [MOI] = 0.37 or 0.018, respectively). On Day 5

pi, the viability of the cells was assessed by adding the MTT reagent (Nakalai Tesque).

Formulation and feeding of drugs and diet

The daily dosages of the drugs were half of those recommended for an adult human, i.e., 300 mg of AZT and 150 mg of 3TC (as Combivir; GlaxoSmithKline, London, UK), 150 mg of Tenofovir disproxil fumarate (TDF, as Viread; Japan Tobacco, Tokyo, Japan), and 400 mg of Lopinavir and 100 mg of Ritonavir (as Kaletra; Abbott). To correlate these dosages for a 4-kg Rhesus macaque with the recommended dosage for an adult human, the body surface area (BSA) of the monkeys was computed as described previously (Du Bois and Du Bois, 1915, 1916). Using BSA and body weight, the *Km* factor for each animal was derived as described (Reagan-Shaw et al., 2008). The dosage for the monkeys corresponded to 3-fold that for an adult human weighing 60 kg. Among the drugs selected, Combivir (AZT/3TC) and Kaletra (LPV/RTV) should be taken twice a day to maintain effective drug concentrations. Therefore, two sets of drug/diet were prepared. Formulation #1 contained AZT, 3TC, LPV, and RTV (150 mg, 75 mg, 200 mg, and 50 mg, respectively), while formulation #2 contained all the drugs in formulation #1 plus TDF (150 mg). Thirty-five grams of primate diet for Old World monkeys (Lab Diet 5048; PMI Nutrition International, Henderson, CO), granulated with a bar blender, was combined with the pulverized drugs. The drug/diet mixture was further mixed with 75 g of squashed banana and formed into a rectangular plate. The formulated drug/diet described above was given to animals in place of their normal diet. Drug/diet formulation #1 was given in the morning and formulation #2 was given 10 h later, at intervals of 10 h and 14 h per day. Seven of the nine Rhesus macaques that were fed the formulated drug/diet ingested 80–90% of total mass within 2 h.

To assess the potential adverse effects of the high-dosage drug administration employed in the current study, serum samples collected from these animals before and during cART were submitted to analyses for the following clinical markers: blood urea nitrogen (BUN), creatinine, total cholesterol, and triglycerides. No substantial fluctuations were observed before and during cART in the values for BUN (average values: for MM491, 16.8 mg/dl; for MM499, 16.0 mg/dl; for MM528, 16.7 mg/dl; and for MM530, 20.9 mg/dl), creatinine (average values: for MM491, 0.5 mg/dl; for MM499, 0.6 mg/dl; for MM528, 0.5 mg/dl; and for MM530, 0.5 mg/dl), and total cholesterol (average values: for MM491, 153 mg/dl; for MM499, 106 mg/dl; for MM528, 109 mg/dl; and for MM530, 132 mg/dl). Nearly all the samples analyzed fell within the normal value ranges for the above-mentioned markers (data not shown). The triglyceride values from all the treated animals, with the exception of MM499, increased upon onset of ART: for MM491, the values ranged from 28 mg/dl at pretreatment to 99 mg/dl at maximum during cART; for MM528, from 21 mg/dl to 58 mg/dl; and for MM530, from 48 mg/dl to 129 mg/dl. The published normal value range for triglycerides in Rhesus macaques is 24–42 mg/dl (Fortman et al., 2001). At autopsy, lipid deposition in the liver was noted in MM530, which exhibited the highest mean level of triglycerides among the three animals, indicative of a certain degree of dysregulation of lipid metabolism. Despite the increase in triglyceride levels, all the treated animals were clinically healthy.

Lopinavir measurement by high-performance liquid chromatography

The drug concentrations in the blood samples were measured by high-performance liquid chromatography (HPLC) as described previously (Frappier et al., 1998), with minor modifications. Briefly, plasma samples collected from two monkeys were subjected to deproteinization by the addition of acetonitrile, and were subsequently loaded onto a HPLC column. The assay conditions were as follows: column, ODS column (150 mm in length and 4.6 mm in diameter; Cadenza); mobile phase, gradient prepared from two solutions (solution A, 0.1% trifluoroacetic acid [TFA] in water; solution B, 0.1% TFA in acetonitrile). The total flow rate was 0.6 ml/min. For detection of the compound, UV absorbance at a wavelength of 215 nm was employed.

Plasma viral RNA measurement

Viral RNA loads in plasma were measured as described previously (Miyake et al., 2006). Briefly, total RNA was extracted from plasma samples with the QIAamp Viral RNA kit (Qiagen, Valencia, CA). The extracted RNA samples were subjected to RT-PCR to amplify the SIV gag region using the TaqMan EZ RT-PCR kit (PerkinElmer, Wellesley, MA). The PCR and detection of products were performed in a Prism 7700 Sequence Detector (Applied Biosystems, Foster City, CA). The primer pair employed for PCR amplification was SIV2-696F (5′-GGAAATTACCCAGTACAACAAA-TAFF-3′) and SIV2-784R (5′-TCTATCAATTTTACCCAggCATTTA-3′). PCR products were detected with a labeled probe, SIV2-731T (5′-Fam-TGTCCACCTGCCATTAAGCCCG-Tamra-3′; Perkin Elmer).

Selected plasma samples from monkeys on cART (at 29, 42, and 52 weeks pi, and at euthanasia) were further subjected to quantitative real-time PCR with a lower detection limit, following the method described by Cline et al., with modifications (Cline et al., 2005). Briefly, 1.5-ml plasma samples were centrifuged at 20,000×*g* for 1 h to sediment virus particles. The pellets were incubated with a mixture of GuHCl (Sigma-Aldrich) and proteinase K (Invitrogen) for 60 min at 37 °C and subsequently incubated with a mixture of GuSCN (Sigma-Aldrich) and glycogen (Roche Applied Science, Indianapolis, IN) for 5 min at room temperature, followed by precipitation with isopropanol. The precipitated RNA fractions were resuspended in water and subjected to RT-PCR, as described above. A standard curve of the reaction was constructed by plotting threshold cycles of serially diluted virus stocks containing known amounts of vRNA extracted in the same manner as the test plasma samples. The detection limit was defined by the standard curve with a correlation coefficient (>0.96) constructed from a set of serial dilutions with reproducible amplification. The detection limit of the assay was consistently <20 copies/ml.

Mathematical modeling and statistical analysis of decay rate

The decline in SIV239 RNA copies in the plasma during cART was evaluated using a mathematical model similar to that developed previously to quantify and analyze the decay of HIV-1 viremia in patients treated with combination anti-retroviral therapy (Perelson et al., 1997). Briefly, two distinct cellular compartments are assumed to contribute to the vRNA. The first compartment consists of $CD4^+$ T cells (i.e., short-lived cells), T, which are infected with a constant, k, die with a rate constant, δ, and have a burst size of N. The second compartment consists of long-lived cells, M, which become infected with a rate constant, k_M, die with a rate, μ_M, and produce p virions per cell. Free virus particles are cleared with a constant, c. Assuming that viral inhibition by cART is 100%, *de novo* infection is completely blocked in this mathematical model. Then, using the parameters explained above, the overall vRNA copies in the plasma can be described by the following equation:

$$V(t) = V_0\left\{\left(1-\frac{NkT_0}{c-\delta}-\frac{c-NkT_0}{c-\mu_M}\right)e^{-ct}+\frac{NkT_0}{c-\delta}e^{\delta t}+\frac{c-NkT_0}{c-\mu_M}e^{\mu M t}\right\}. \quad (1)$$

Here, V_0 and T_0 are the steady-state level of viral load and $CD4^+$ T cells count before HAART, respectively. The derivation of Eq. (1) is explained in detail elsewhere (Perelson and Nelson, 1999). To fit the plasma viremia data with the two-compartment model, we estimated the parameters, δ, μ_M, and a composite parameter, NkT_0, employing